

Dynamical quasiparticles properties and effective interactions in the sQGP

W. Cassing^{a,*}

^a*Institut für Theoretische Physik, Universität Giessen, Heinrich-Buff-Ring 16,
D-35392 Giessen, Germany*

Abstract

Dynamical quasiparticle properties are determined from lattice QCD along the line of the Peshier model for the running strong coupling constant in case of three light flavors. By separating time-like and space-like quantities in the number density and energy density the effective degrees of freedom in the gluon and quark sector may be specified from the time-like densities. The space-like parts of the energy densities are identified with interaction energy (or potential energy) densities. By using the time-like parton densities (or scalar densities) as independent degrees of freedom - instead of the temperature T and chemical potential μ_q as Lagrange parameters - variations of the potential energy densities with respect to the time-like gluon and/or fermion densities lead to effective mean-fields for time-like gluons and quarks as well as to effective gluon-gluon, quark-gluon and quark-quark (quark-antiquark) interactions. The latter dynamical quantities are found to be approximately independent on the quark chemical potential μ_q and thus well suited for an implementation in off-shell parton transport approaches. Results from the dynamical quasiparticle model (DQPM) in case of two dynamical light quark flavors are compared to lattice QCD calculations for the net quark density $\rho_q(T, \mu_q)$ as well as for the 'back-to-back' differential dilepton production rate by $q - \bar{q}$ annihilation. The DQPM is found to pass the independent tests.

Key words: Quark gluon plasma, General properties of QCD, Relativistic heavy-ion collisions

PACS: 12.38.Mh, 12.38.Aw, 25.75.-q

* corresponding author

Email address: Wolfgang.Cassing@theo.physik.uni-giessen.de (W. Cassing).

1 Introduction

The 'Big Bang' scenario implies that in the first micro-seconds of the universe the entire system has emerged from a partonic system of quarks, antiquarks and gluons – a quark-gluon plasma (QGP) – to color neutral hadronic matter consisting of interacting hadronic states (and resonances) in which the partonic degrees of freedom are confined. The nature of confinement and the dynamics of this phase transition has motivated a large community for several decades (cf. [1–3] and Refs. therein). Early concepts of the QGP were guided by the idea of a weakly interacting system of partons since the entropy density s and energy density ϵ were found in lattice QCD to be close to the Stefan Boltzmann (SB) limit for a relativistic noninteracting system [4]. However, experimental observations at the Relativistic Heavy Ion Collider (RHIC) indicated that the new medium created in ultrarelativistic Au+Au collisions was interacting more strongly than hadronic matter and consequently this notion had to be given up. Moreover, in line with earlier theoretical studies in Refs. [5–7] the medium showed phenomena of an almost perfect liquid of partons [8,9] as extracted from the strong radial expansion and elliptic flow of hadrons as well the scaling of the elliptic flow with parton number *etc.* All the latter collective observables have been severely underestimated in conventional string/hadron transport models [10–12] whereas hydrodynamical approaches did quite well in describing (at midrapidity) the collective properties of the medium generated during the early times for low and moderate transverse momenta [13,14]. The question about the constituents and properties of this QGP liquid is discussed controversially in the literature (cf. Refs. [15–17]) and practically no dynamical concepts are available to describe the dynamical freezeout of partons to color neutral hadrons that are finally observed experimentally. Since the partonic system appears to interact more strongly than even hadronic systems the notation strong QGP (sQGP) has been introduced in order to distinguish from the dynamics known from perturbative QCD (pQCD).

Lattice QCD (lQCD) calculations provide some guidance to the thermodynamic properties of the partonic medium close to the transition at a critical temperature T_c up to a few times T_c , but lQCD calculations for transport coefficients presently are not accurate enough [18] to allow for firm conclusions. Furthermore, it is not clear whether the partonic system really reaches thermal and chemical equilibrium in ultrarelativistic nucleus-nucleus collisions [19] such that nonequilibrium models are needed to trace the entire collision history. The available string/hadron transport models [20–22] partly fail - as pointed out above - nor do partonic cascade simulations [23–26] (propagating massless partons) sufficiently describe the reaction dynamics when employing cross sections from perturbative QCD. Some models, e.g. the Multiphase Transport Model AMPT [27], employ strong enhancement factors for the cross sections, however, use only on-shell massless partons in the partonic phase as in Ref. [24]. The same problem comes about in the parton cascade model of Ref. [28] where additional $2 \leftrightarrow 3$ processes like $gg \leftrightarrow ggg$ are incorporated but massless partons are considered.

On the other hand it is well known that strongly interacting quantum systems require descriptions in terms of propagators D with sizeable selfenergies Π for the relevant degrees of freedom. Whereas the real part of the selfenergies can be related to mean-field potentials, the imaginary parts of Π provide information about the lifetime and/or reaction rate of time-like 'particles' [6]. In principle, off-shell transport equations are available in the literature [29–31], but have been applied only to dynamical problems where the width of the quasiparticles stays moderate with respect to the pole mass [32]. On the other hand, the studies of Peshier [33,34] indicate that the effective degrees of freedom in a partonic phase should have a width γ in the order of the pole mass M already slightly above T_c . This opens up the problem how to interpret/deal with the space-like part of the distribution functions and how to 'propagate' effective degrees in space-time in equilibrium as well as out of equilibrium.

Some elementary steps in answering these questions have been presented in a preceding work [35] where the pure Yang-Mills sector of QCD has been addressed in the Dynamical QuasiParticle model (DQPM) of Peshier [33,34]. In the latter work it could be demonstrated that the DQPM allows for a rather simple and transparent interpretation of QCD thermodynamics and leads to effective strongly interacting gluonic degrees of freedom that may be propagated in off-shell transport approaches as e.g. in Ref. [36]. The present study is an extension of the work in Ref. [35] to three light quark flavors ($q = u, d, s$) and to finite quark chemical potential μ_q in order to determine the effective partonic degrees of freedom, their mean-fields and interactions for a practical implementation in the off-shell parton transport model PHSD¹ [36]. First results of the PHSD approach for dynamical phase trajectories in central Au+Au collisions have been presented in Ref. [37].

The outline of the paper is as follows: After a short recapitulation of the dynamical quasiparticle model with dynamical quarks in Section 2 novel results on the space-like and time-like parts of observables are presented that allow for a transparent physical interpretation. In Section 3 we will examine derivatives of the space-like part of the quasiparticle energy density with respect to the time-like densities which provides information on partonic mean-fields and their effective interaction strength. An extension of the model to finite quark chemical potentials is given in Section 4 including a comparison of the net quark density $\rho_q(T, \mu_q)$ with lQCD calculations in the two flavor case. In Section 5 the 'back-to-back' dilepton production rate is calculated in the DQPM and compared to respective lQCD calculations again for two dynamical quark flavors. A summary and short discussion closes this work in Section 6.

¹ Parton-Hadron-String Dynamics

2 Off-shell elements in the DQPM

2.1 Reminder of the DQPM

The dynamical quasiparticle model adopted here goes back to Peshier [33,34] and starts with the entropy density in the quasiparticle limit [34,38–40],

$$\begin{aligned}
s^{dqp} = & -d_g \int \frac{d\omega}{2\pi} \frac{d^3p}{(2\pi)^3} \frac{\partial n_B}{\partial T} \left(\text{Im} \ln(-\Delta^{-1}) + \text{Im} \Pi \text{Re} \Delta \right) \\
& -d_q \int \frac{d\omega}{2\pi} \frac{d^3p}{(2\pi)^3} \frac{\partial n_F((\omega - \mu_q)/T)}{\partial T} \left(\text{Im} \ln(-S_q^{-1}) + \text{Im} \Sigma_q \text{Re} S_q \right), \\
& -d_{\bar{q}} \int \frac{d\omega}{2\pi} \frac{d^3p}{(2\pi)^3} \frac{\partial n_F((\omega + \mu_q)/T)}{\partial T} \left(\text{Im} \ln(-S_{\bar{q}}^{-1}) + \text{Im} \Sigma_{\bar{q}} \text{Re} S_{\bar{q}} \right),
\end{aligned} \tag{1}$$

where $n_B(\omega/T) = (\exp(\omega/T) - 1)^{-1}$ and $n_F((\omega - \mu_q)/T) = (\exp((\omega - \mu_q)/T) + 1)^{-1}$ denote the Bose and Fermi distribution functions, respectively, while $\Delta = (P^2 - \Pi)^{-1}$, $S_q = (P^2 - \Sigma_q)^{-1}$ and $S_{\bar{q}} = (P^2 - \Sigma_{\bar{q}})^{-1}$ stand for scalar quasiparticle propagators of gluons g , quarks q and antiquarks \bar{q} . The degeneracy factor for gluons is $d_g = 2(N_c^2 - 1) = 16$ while for quarks q and antiquarks \bar{q} we get $d_q = d_{\bar{q}} = 2N_c N_f 7/8 = 15.25$ for three flavors N_f . In (1) Π and $\Sigma = \Sigma_q \approx \Sigma_{\bar{q}}$ denote the quasiparticle selfenergies. In principle, Π as well as Δ are Lorentz tensors and should be evaluated in a nonperturbative framework. The DQPM treats these degrees of freedom as independent scalar fields with a scalar selfenergy Π . In case of the fermions $S_q, S_{\bar{q}}$ and $\Sigma_q, \Sigma_{\bar{q}}$ (for q and \bar{q}) have Lorentz scalar and vector contributions but only scalar terms are kept in (1) for simplicity which are assumed to be identical for quarks and antiquarks. Note that one has to treat quarks and antiquarks separately in (1) as their abundance differs at finite quark chemical potential μ_q .

Since the nonperturbative evaluation of the propagators and selfenergies is a formidable task (and presently not solved) a more practical procedure is to use physically motivated *Ansätze* with Lorentzian spectral functions for quarks² and gluons,

$$\rho(\omega) = \frac{\gamma}{E} \left(\frac{1}{(\omega - E)^2 + \gamma^2} - \frac{1}{(\omega + E)^2 + \gamma^2} \right), \tag{2}$$

and to fit the few parameters to results from lQCD. With the convention $E^2(\mathbf{p}) = \mathbf{p}^2 + M^2 - \gamma^2$, the parameters M^2 and γ are directly related to the real and imaginary parts of the corresponding (retarded) self-energy, e.g. $\Pi = M^2 - 2i\gamma\omega$ in case of the 'scalar' gluons.

² In the following the abbreviation is used that 'quarks' denote quarks and antiquarks if not specified explicitly.

Following [34] the quasiparticle mass (squared) for gluons is assumed to be given by the thermal mass in the asymptotic high-momentum regime, i.e.

$$M^2(T) = \frac{g^2}{6} \left((N_c + \frac{1}{2}N_f) T^2 + \frac{N_c}{2} \sum_q \frac{\mu_q^2}{\pi^2} \right), \quad (3)$$

and for quarks (assuming vanishing constituent masses) as,

$$m^2(T) = \frac{N_c^2 - 1}{8N_c} g^2 \left(T^2 + \frac{\mu_q^2}{\pi^2} \right), \quad (4)$$

with a running coupling (squared),

$$g^2(T/T_c) = \frac{48\pi^2}{(11N_c - 2N_f) \ln(\lambda^2(T/T_c - T_s/T_c)^2)}, \quad (5)$$

which permits for an enhancement near T_c [41–43]. Here $N_c = 3$ stands for the number of colors while N_f denotes the number of flavors and μ_q the quark chemical potentials. The parameters $\lambda = 2.42$ and $T_s/T_c = 0.46$ are adopted from [34]. As demonstrated in Fig. 1 of Ref. [35] this functional form for the strong coupling $\alpha_s = g^2/(4\pi)$ is in accordance with the lQCD calculations of Ref. [44] for the long range part of the $q - \bar{q}$ potential.

The width for gluons and quarks (for $\mu_q = 0$) is adopted in the form [45]

$$\gamma_g(T) = N_c \frac{g^2 T}{8\pi} \ln \frac{2c}{g^2}, \quad \gamma_q(T) = \frac{N_c^2 - 1}{2N_c} \frac{g^2 T}{8\pi} \ln \frac{2c}{g^2}. \quad (6)$$

where $c = 14.4$ (from Ref. [6]) is related to a magnetic cut-off. Note that in case of vanishing number of flavors $N_f = 0$ the expressions for the masses and the coupling reduce to those employed for the pure Yang-Mills sector [34,35].

The physical processes contributing to the width γ_g are both $gg \leftrightarrow gg$, $gq \leftrightarrow gq$ scattering as well as splitting and fusion reactions $gg \leftrightarrow g$, $gg \leftrightarrow ggg$, $ggg \leftrightarrow gggg$ or $g \leftrightarrow q\bar{q}$ etc. On the fermion side elastic fermion-fermion scattering $pp \leftrightarrow pp$, where p stands for a quark q or antiquark \bar{q} , fermion-gluon scattering $pg \leftrightarrow pg$, gluon bremsstrahlung $pp \leftrightarrow pp + g$ or quark-antiquark fusion $q\bar{q} \leftrightarrow g$ etc. emerge. Note, however, that the explicit form of (6) is derived for hard two-body scatterings only. It is worth to point out that the ratio of the masses to their widths $\sim g \ln(2c/g^2)$ approaches zero only asymptotically for $T \rightarrow \infty$ such that the width of the quasiparticles is comparable to the pole mass slightly above T_c up to all terrestrial energy scales.

Within the DQPM the real and imaginary parts of the propagators Δ and S now are fixed and the entropy density (1) can be evaluated numerically once the free

parameters in (5) are determined. In the following we will assume 3 light quark flavors $N_f = 3$. Since the presently available unquenched IQCD calculations (for three flavors) for the entropy density are still accompanied with rather large error bars the parameters of the DQPM are taken the same as in the pure Yang-Mills sector: $\lambda = 2.42$, $T_s/T_c = 0.46$ as determined in Ref. [6]. This is legitimate since an approximate scaling of thermodynamic quantities from IQCD is observed when dividing by the number of degrees of freedom and scaling by the individual critical temperature T_c which is a function of the different number of parton species [46]. However, these parameters will have to be refitted once more accurate 'lattice data' become available.

The resulting values for the gluon and quark masses - multiplied by T_c/T - are displayed in Fig. 1 (for $\mu_q = 0$) by the solid lines while the gluon and quark width (γ_g, γ_q) - multiplied by T_c/T - are displayed in terms of the dashed lines as a function of T/T_c . The actual numbers are found to be quite similar as in the pure Yang Mills case [6,33,34] and imply very 'broad' quasiparticles already slightly above T_c . For $\mu_q = 0$ the ratio $\gamma_q/\gamma_g = 4/9$ is the same as for the ratio of the squared masses $m^2/M^2 = 4/9$ and reflects the ratio of the Casimir eigenvalues in color space. Consequently the ratio of the width to the pole mass is smaller for quarks (antiquarks) than for gluons in the whole temperature range.

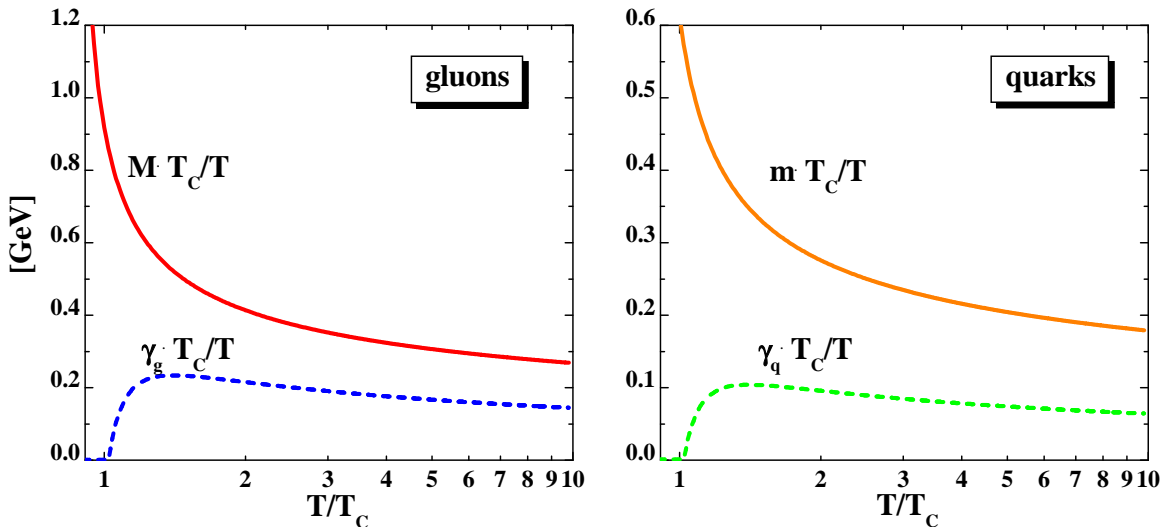


Fig. 1. The mass M (solid red line) and width γ_g (dashed blue line) for gluons (l.h.s.) and the mass m (solid orange line) and width γ_q (dashed green line) for quarks (r.h.s.) as a function of T/T_c in the DQPM for $\lambda = 2.42$, $T_s/T_c = 0.46$, and $c = 14.4$ (for $\mu_q = 0$). All quantities have been multiplied by the dimensionless factor T_c/T .

In order to fix the scale T_c , which is not specified so far, one may directly address unquenched IQCD calculations (for 3 light flavors). However, here the situation is presently controversial between different groups (cf. Refs. [47,48] and the discussion therein). An alternative way is to calculate the pressure P from the thermodynamical

relation,

$$s = \frac{\partial P}{\partial T} , \quad (7)$$

by integration of the entropy density s over T , where one may tacitly identify the 'full' entropy density s with the quasiparticle entropy density s^{dqp} (1). Since for $T < T_c$ the DQPM entropy density drops to zero (with decreasing T) due to the high quasiparticle masses and the width γ vanishes as well (cf. Fig. 1) the integration constant may be assumed to be zero in the DQPM which focusses on the quasiparticle properties above T_c .

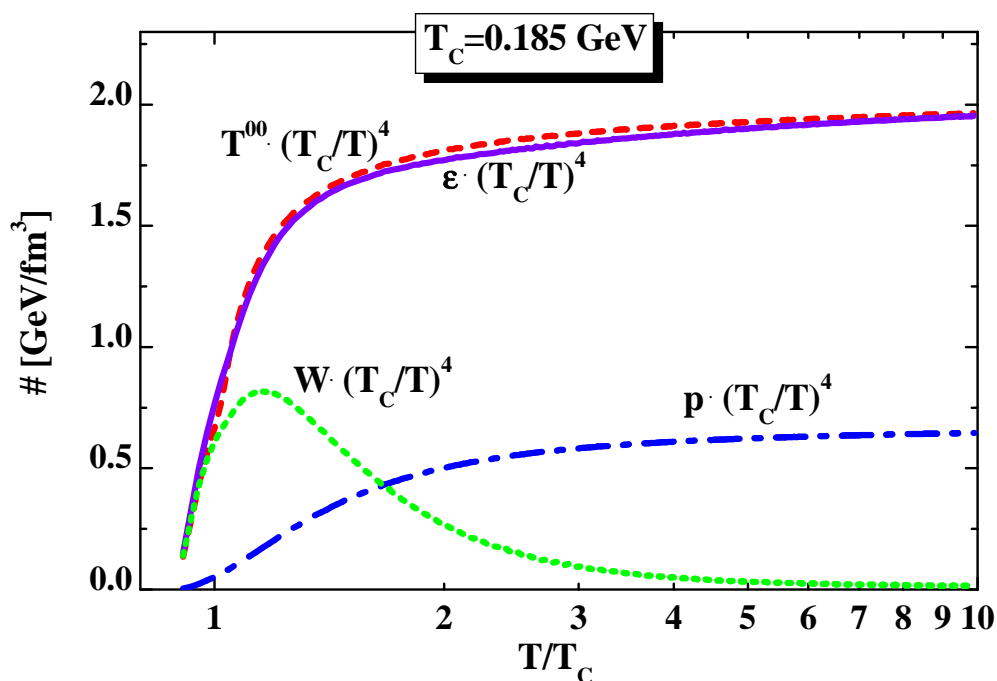


Fig. 2. The DQPM results for $\epsilon(T/T_c)(T_c/T)^4$ (solid violet line), $P(T/T_c)(T_c/T)^4$ (blue dash-dotted line) and the interaction measure $W(T/T_c)(T_c/T)^4$ (9) (green dotted line). Note the logarithmic scale in T/T_c . The energy density ϵ (8) practically coincides with the quasiparticle energy density T^{00} from (16) (dashed red line).

The energy density ϵ then follows from the thermodynamical relation [41,49]

$$\epsilon = Ts - P \quad (8)$$

and thus is also fixed by the entropy $s(T)$ as well as the interaction measure

$$W(T) := \epsilon(T) - 3P(T) = Ts - 4P \quad (9)$$

that vanishes for massless and noninteracting degrees of freedom.

The actual results for $\epsilon \cdot (T_c/T)^4$ are displayed in Fig. 2 (solid violet line), $P \cdot (T_c/T)^4$ (blue dash-dotted line) as well as the interaction measure $W \cdot (T_c/T)^4$ (9) (green dotted line) and show the typical pattern from lQCD calculations [46]. The scale T_c may now be fixed (estimated) by requiring that the critical energy density $\epsilon(T_c)$ is roughly the same for the pure Yang-Mills case as for the full theory with dynamical quarks in line with the approximate scaling of lQCD [46]. Since $\epsilon(T_c)$ in the Yang Mills sector is about $1 \text{ GeV}/\text{fm}^3$ (cf. [35]) the scaled energy density $\epsilon(T/T_c)$ from Fig. 2 can be employed to fix the critical temperature $T_c \approx 0.185 \text{ GeV}$. This leads to the 'thumb rule' $\epsilon \approx 2 (T/T_c)^4 [\text{GeV}/\text{fm}^3]$ for $T > 1.2T_c$ which is roughly fulfilled according to Fig. 2.

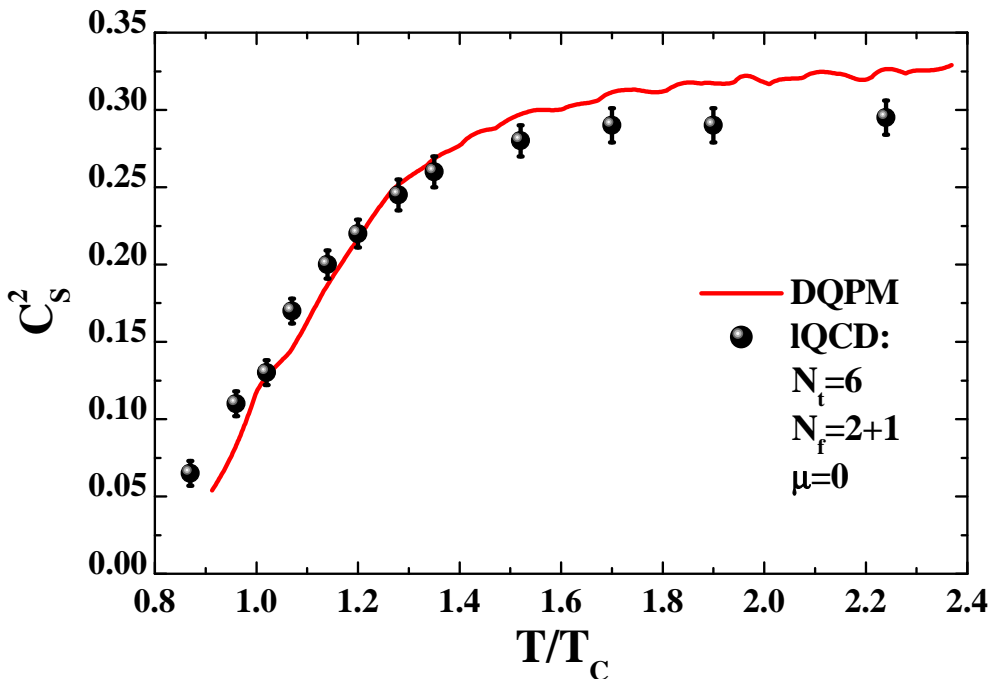


Fig. 3. The DQPM results for the sound velocity (squared) (10) as a function of T/T_c in comparison to the IQCD results from Ref. [50].

A first test of the DQPM in comparison to lQCD calculations is given for the sound velocity (squared),

$$c_s^2 = \frac{dP}{d\epsilon} , \quad (10)$$

which does not depend on the absolute (uncertain) scale of T_c . This comparison is shown in Fig. 3 by the solid line where the lQCD results have been taken from Ref. [50] and correspond to $N_f = 2 + 1$ with $N_t = 6$. The DQPM is seen to reproduce

the drop in c_s^2 close to T_c within errorbars and to reach the asymptotic value $c_s^2 = 1/3$ approximately for $T > 2 T_c$. This comparison, however, has to be taken with some care since the DQPM assumes massless current quarks whereas the lQCD calculations employ finite quark masses.

2.2 Time-like and space-like quantities

For the further analysis of the DQPM it is useful to introduce the shorthand notations (extending [6,35])

$$\tilde{\text{Tr}}_g^\pm \dots = d_g \int \frac{d\omega}{2\pi} \frac{d^3p}{(2\pi)^3} 2\omega \rho_g(\omega) \Theta(\omega) n_B(\omega/T) \Theta(\pm P^2) \dots \quad (11)$$

$$\tilde{\text{Tr}}_q^\pm \dots = d_q \int \frac{d\omega}{2\pi} \frac{d^3p}{(2\pi)^3} 2\omega \rho_q(\omega) \Theta(\omega) n_F((\omega - \mu_q)/T) \Theta(\pm P^2) \dots$$

$$\tilde{\text{Tr}}_{\bar{q}}^\pm \dots = d_{\bar{q}} \int \frac{d\omega}{2\pi} \frac{d^3p}{(2\pi)^3} 2\omega \rho_{\bar{q}}(\omega) \Theta(\omega) n_F((\omega + \mu_q)/T) \Theta(\pm P^2) \dots$$

with $P^2 = \omega^2 - \mathbf{p}^2$ denoting the invariant mass squared. The quark and antiquark degrees of freedom, i.e. $2d_q = 31.5$, are consequently by roughly a factor of two more abundant than the gluonic degrees of freedom. The $\Theta(\pm P^2)$ function in (11) separates time-like quantities from space-like quantities and can be inserted for any observable of interest. Note, however, that not all space-like quantities have a direct physical interpretation.

We note in passing that the entropy density (1) is dominated by the time-like contributions for quarks and gluons and shows only minor space-like parts (cf. Refs. [34,35]). Furthermore, the entropy density from the DQPM is only 10 - 15 % smaller than the Stefan Boltzmann entropy density s_{SB} for $T > 2 T_c$ as in case of lQCD [4]. Since these results provide no novel information an explicit representation is discarded.

Further quantities of interest are the 'quasiparticle densities'

$$N_g^\pm(T) = \tilde{\text{Tr}}_g^\pm 1, \quad N_q^\pm(T) = \tilde{\text{Tr}}_q^\pm 1, \quad N_{\bar{q}}^\pm(T) = \tilde{\text{Tr}}_{\bar{q}}^\pm 1, \quad (12)$$

that correspond to the time-like (+) and space-like (-) parts of the integrated distribution functions. Note that only the time-like integrals over space have a particle number interpretation. In QED this corresponds e.g. to time-like photons (γ^*) which are virtual in intermediate processes but may also be seen asymptotically by dileptons (e.g. e^+e^- pairs) due to the decay $\gamma^* \rightarrow e^+e^- (\mu^+ + \mu^-)$ [20].

Scalar densities for quarks and gluons - only defined in the time-like sector - are given by

$$N_g^s(T) = \tilde{\text{Tr}}_g^+ \left(\frac{\sqrt{P^2}}{\omega} \right), \quad N_q^s(T) = \tilde{\text{Tr}}_q^+ \left(\frac{\sqrt{P^2}}{\omega} \right), \quad N_{\bar{q}}^s(T) = \tilde{\text{Tr}}_{\bar{q}}^+ \left(\frac{\sqrt{P^2}}{\omega} \right) \quad (13)$$

and have the virtue of being Lorentz invariant.

Before coming to the actual results for the quantities (12) and (13) it is instructive to have a look at the integrand in the quark density (12) which reads as (in spherical momentum coordinates with angular degrees of freedom integrated out)

$$I(\omega, p) = \frac{d_q}{2\pi^3} p^2 \omega \rho_q(\omega, p^2) n_F((\omega - \mu_q)/T). \quad (14)$$

Here the integration is to be taken over ω and p from 0 to ∞ . The integrand $I(\omega, p)$ is shown in Fig. 4 for $T = 1.05T_c$ (l.h.s.) and $T = 3T_c$ (r.h.s.) ($\mu_q = 0$) in terms of contour lines spanning both one order of magnitude. For the lower temperature the quark mass is about 0.55 GeV and the width $\gamma \approx 0.034$ GeV such that the quasiparticle properties are close to an on-shell particle. In this case the integrand $I(\omega, p)$ is essentially located in the time-like sector and the integral over the space-like sector is almost negligible. This situation changes for $T = 3T_c$ where the mass is about 0.7 GeV while the width increases to $\gamma \approx 0.25$ GeV. As one observes from the r.h.s. of Fig. 4 the maximum of the integrand is shifted towards the line $\omega = p$ and higher momentum due to the increase in temperature by about a factor of three; furthermore, the distribution reaches far out in the space-like sector due to the Fermi factor $n_F(\omega/T)$ which favors small ω . Thus the relative importance of the time-like (+) part to the space-like (-) part is dominantly controlled by the width γ - relative to the pole mass - which determines the fraction of N_q^- with negative invariant mass squared ($P^2 < 0$) relative to the time-like part N_q^+ ($P^2 > 0$).

The actual results for the different 'densities' (multiplied by $(T_c/T)^3$) are displayed in Fig. 5 for gluons (l.h.s.) and quarks (r.h.s.) including the antiquarks. The lower (magenta) lines represent the scalar densities N^s , the red solid lines the time-like densities N^+ , the green lines the quantities N^- while the thick solid blue lines are the sum $N = N^+ + N^-$ as a function of T/T_c (assuming $T_c = 0.185$ GeV). It is seen that N^+ is substantially smaller than N^- in case of gluons in the temperature range $1.1 \leq T/T_c \leq 10$. Except for an overall scale factor the result for gluons is practically the same as in the pure Yang-Mills case (cf. Fig. 3 in Ref. [35]). The quantity N follows closely the Stefan Boltzmann limit N_{SB} for a massless noninteracting system of bosons which is given in Fig. 5 (l.h.s.) by the upper dash-dotted line. Though N differs by less than 20% from the Stefan Boltzmann (SB) limit for $T > 2T_c$ the physical interpretation is essentially different! Whereas in the SB limit all gluons move on the light cone without interactions only a small fraction of gluons can be attributed to quasiparticles with density N^+ within the DQPM that propagate

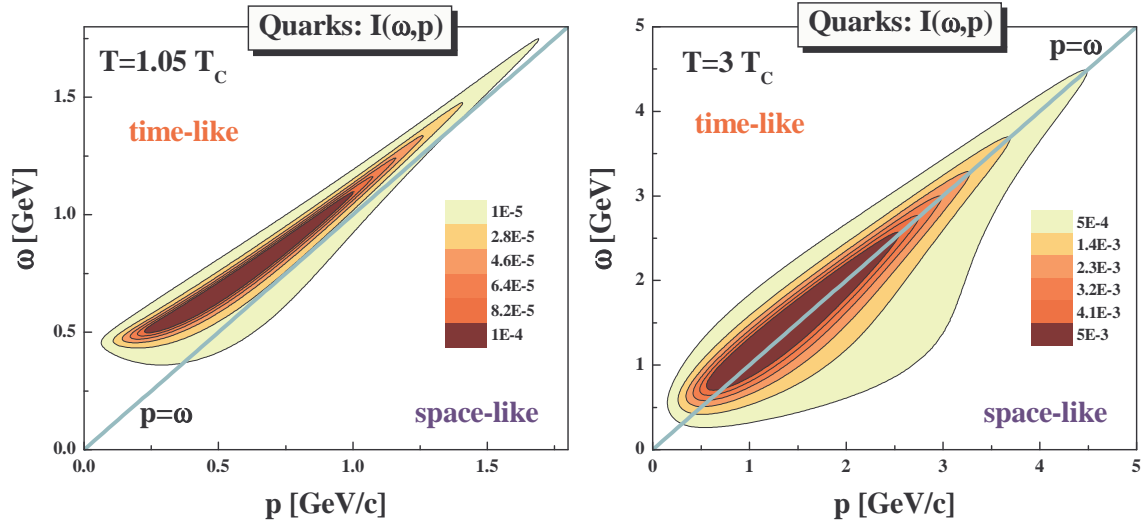


Fig. 4. The integrand $I(\omega, p)$ (14) as a function of ω and p for quarks at temperatures $T = 1.05 T_c$ (l.h.s.) and $T = 3 T_c$ (r.h.s.). At $T = 1.05 T_c$ (l.h.s.) the quasiparticle mass amounts to $m \approx 0.55$ GeV and the width to $\gamma_q \approx 0.034$ GeV while at $T = 3 T_c$ (r.h.s.) $m \approx 0.7$ GeV and $\gamma_q \approx 0.25$ GeV. The contour lines in both figures extend over one order of magnitude. Note that for a convergence of the integrals (12) the upper limits for ω and p have to be increased by roughly an order of magnitude compared to the area shown in the figure.

within the lightcone. The space-like part N^- corresponds to 'gluons' exchanged in t -channel scattering processes and thus cannot be propagated explicitly in off-shell transport approaches without violating causality and/or Lorentz invariance. In case of quarks (or antiquarks) the results are qualitatively similar but now the time-like part N^+ comes closer to the space-like part N^- since the ratio of the width to the pole mass (γ_q/m) is smaller than the corresponding ratio for gluons as stated above. Furthermore, the quantity N is closer to the respective SB limit (for massless fermions) due to the lower effective mass of the quarks. In this respect the quarks and antiquarks are closer to (but still far from) the massless on-shell quasiparticle limit.

The scalar densities N^s (lower magenta lines) follow smoothly the time-like densities N^+ (for gluons as well as quarks+antiquarks) as a function of temperature and uniquely relate to the corresponding time-like densities N^+ or the temperature T in thermal equilibrium.

The separation of N^+ and N^- so far has no direct dynamical implications except for the fact that only the fraction N^+ can explicitly be propagated in transport models as argued above. Following Ref. [35] we, furthermore, consider the energy densities,

$$T_{00,x}^\pm(T) = \tilde{\text{Tr}}_x^\pm \omega , \quad (15)$$

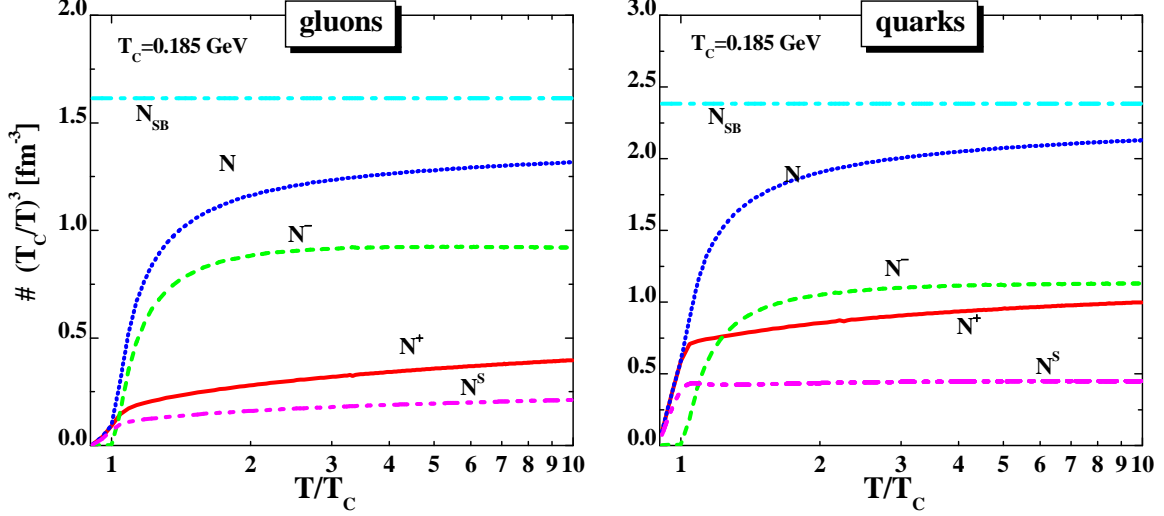


Fig. 5. The various 'densities' (12) for gluons (l.h.s.) and quarks (r.h.s.) including antiquarks (at $\mu_q = 0$). The lower magenta lines represent the scalar densities N^s , the red solid lines the time-like densities N^+ , the green lines the quantities N^- while the thick solid blue lines are the sum $N = N^+ + N^-$ as a function of T/T_c . The upper dash-dotted lines display the Stefan Boltzmann limits N_{SB} for reference. All densities are multiplied by the dimensionless factor $(T_c/T)^3$ to divide out the leading scaling with temperature.

that specify time-like and space-like contributions to the quasiparticle energy densities ($x = g, q, \bar{q}$).

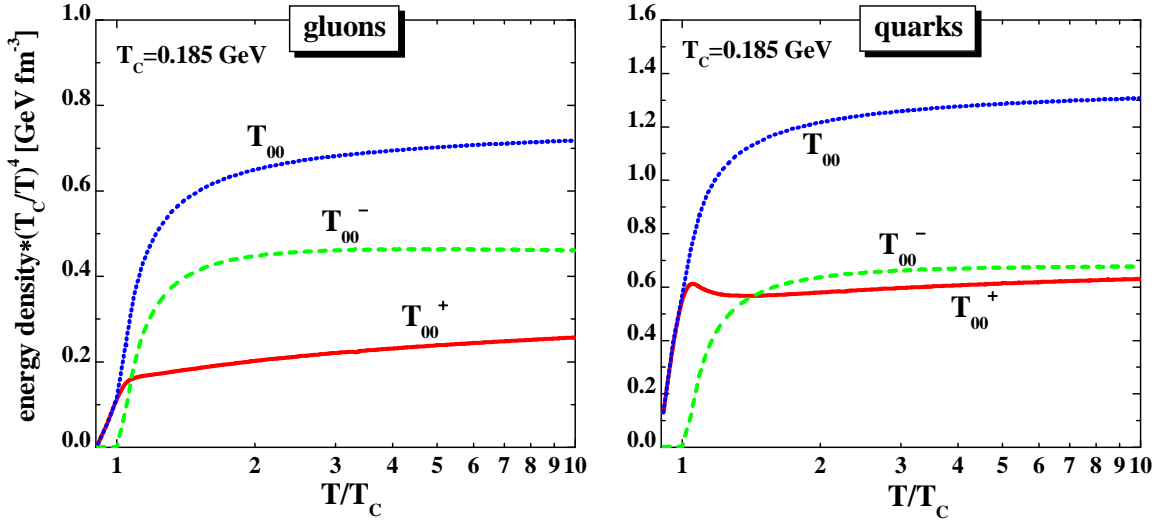


Fig. 6. The time-like energy density T_{00}^+ (red solid line), the space-like energy density T_{00}^- (dashed green line) and their sum $T_{00} = T_{00}^+ + T_{00}^-$ (upper blue line) as a function of T/T_c for gluons (l.h.s.) and quarks (+ antiquarks) (r.h.s.). All densities are multiplied by the dimensionless factor $(T_c/T)^4$.

The result for the quasiparticle energy densities T_{00}^+ and T_{00}^- are displayed in Fig. 6 for gluons (l.h.s.) and quarks+antiquarks (r.h.s.) as a function of T/T_c . All quantities have been multiplied by the dimensionless factor $(T_c/T)^4$ in order to divide out

the leading temperature dependence. The lower red solid lines show the time-like components T_{00}^+ while the dashed green lines display the space-like parts T_{00}^- which dominate over the time-like parts except in the vicinity of T_c . The general behaviour for the scaled energy densities T_{00}^\pm is similar as for the 'densities' N^\pm given in Fig. 5 since the extra factor ω in the integrand does not change significantly the time-like and space-like parts. As in Ref. [35] the space-like parts are interpreted as potential energy densities while the time-like fractions are the gluon and quark quasiparticle contributions which propagate within the lightcone.

Summing up the time-like and space-like contributions for gluons, quarks and antiquarks we obtain the total energy density T^{00} ,

$$T^{00} = T_{00,g}^+ + T_{00,g}^- + T_{00,q}^+ + T_{00,q}^- + T_{00,\bar{q}}^+ + T_{00,\bar{q}}^- , \quad (16)$$

which is displayed in Fig. 2 by the dashed red line (scaled by T_c/T)⁴. As in case of the pure Yang-Mills system in Ref. [35] the quantity T^{00} practically coincides with the energy density ϵ (8) obtained from the thermodynamical relations. Small differences of less than 5% show up which indicates that the DQPM in its present formulation is not fully consistent in the thermodynamical sense. Since these differences are small on an absolute scale and significantly smaller than differences between present independent IQCD calculations for 3 quark flavors one may consider $T^{00}(T) \approx \epsilon(T)$ and separate the kinetic energy densities T_{00}^+ from the potential energy densities T_{00}^- as a function of the temperature T or - in equilibrium - as a function of the scalar densities N^s or time-like densities N^+ , respectively.

It is instructive to show the potential energies per degree of freedom $V_{gg}/N_g^+ = T_{00,g}^-/N_g^+$ and $V_{qq}/N_q^+ = T_{00,q}^-/N_q^+$ as a function of T/T_c . The corresponding quantities are displayed in Fig. 7 (l.h.s.) multiplied by T_c/T in terms of the solid red line and the dot-dashed blue line. It is seen that the potential energies per degree of freedom steeply rise in the vicinity of T_c and then increase approximately linear with temperature T . As expected from the larger width of the gluons the latter also show a potential energy per degree of freedom which is roughly a factor of two larger than the corresponding quantity for quarks (antiquarks). Consequently rapid changes in the temperature (or density) - as in the expansion of the fireball in ultrarelativistic nucleus-nucleus collisions - are accompanied by a dramatic change in the potential energy density and thus to a violent acceleration of the quasiparticles. It is speculated here that the large collective flow of practically all hadrons seen at RHIC [8] might be attributed to the early strong partonic forces expected from the DQPM.

Furthermore, the plasma parameter Γ defined by the ratio of the average potential energy per particle to the average kinetic energy per particle,

$$\Gamma_g = \frac{V_{gg}}{T_{kin,g}} , \quad \Gamma_q = \frac{V_{qq}}{T_{kin,q}} , \quad (17)$$

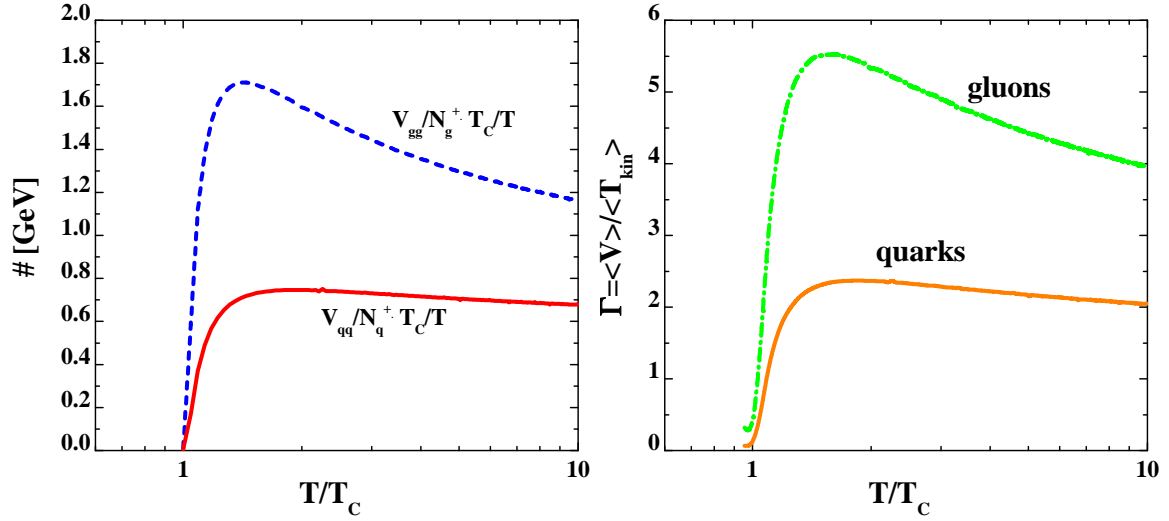


Fig. 7. l.h.s.: The potential energies per degree of freedom for gluons $V_{gg}/N_g^+ = T_{00,g}^-/N_g^+$ (dashed blue line) and for quarks (antiquarks) $V_{qq}/N_q^+ = T_{00,q}^-/N_q^+$ (solid red line) as a function of T/T_c . All energies are multiplied by the dimensionless factor (T_c/T) . r.h.s.: The plasma parameter Γ (17) for gluons (dot-dashed green line) and quarks (solid orange line) as a function of T/T_c . Note that $\Gamma \approx 1 - 2$ separates a gas phase from a liquid phase in case of Lenard-Jones type of interactions.

is displayed in the r.h.s. of Fig. 7 for gluons (dot-dashed green line) and quarks (solid orange line) as a function of T/T_c . Here the kinetic energy densities are evaluated as [6]

$$T_{kin,g} = \tilde{T}r_g^+(\omega - \sqrt{P^2}), \quad T_{kin,q} = \tilde{T}r_q^+(\omega - \sqrt{P^2}). \quad (18)$$

The presents results clearly indicate that the plasma parameters Γ_g, Γ_q are larger than unity for both quarks and gluons up to 10 T_c (except for the vicinity of T_c) such that the system should be in a liquid phase provided that some attractive interaction between the constituents persists. Note that the present evaluation of the plasma parameter Γ is entirely carried out within the DQPM and no longer based on estimates for the potential energy as in Refs. [5,6]. Whereas in the earlier estimates Γ_g was dropping with temperature and becoming lower than unity for $T > 4 T_c$ [6] the present results indicate that the sQGP should persist for a much larger range in temperature (or energy density) and thus also show up in nucleus-nucleus collisions at Large Hadron Collider (LHC) energies. Consequently, a partonic liquid is expected to be seen also at LHC energies and as a consequence the observed scaling of elliptic flow of practically all hadrons with the number of constituent quarks (as seen at RHIC) should persist also at LHC.

3 Selfenergies and effective interactions of time-like quasiparticles

Since in transport dynamical approaches there are no thermodynamical Lagrange parameters like the inverse temperature $\beta = T^{-1}$ or the quark chemical potential μ_q , which have to be introduced in thermodynamics in order to specify the average values of conserved quantities (or currents in the relativistic sense), derivatives of physical quantities with respect to the scalar densities N_x^s (or time-like densities N_x^+) ($x = g, q, \bar{q}$) are considered in the following (cf. Refs. [35,51]).

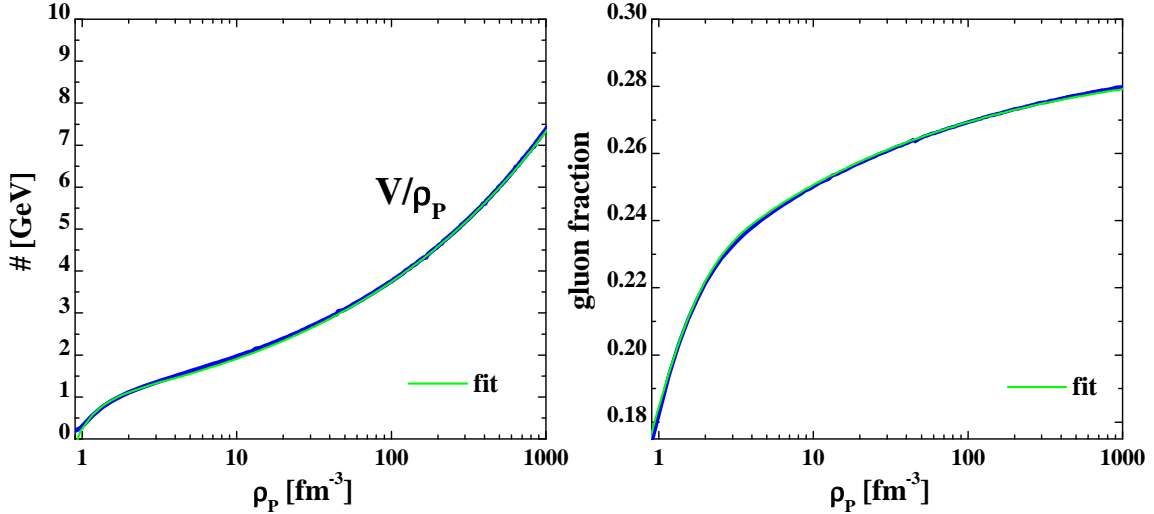


Fig. 8. The parton potential energy density V (19) - divided by the parton density ρ_p - from the DQPM (l.h.s., blue line) as a function of the parton density ρ_p (20). The functional form of $V(\rho_p)$ is well reproduced by the expression (22) when divided by ρ_p (green line) such that the lines cannot be separated by eye. The r.h.s. shows the gluon fraction α (20) from the DQPM (dark blue line) as a function of ρ_p together with the fit (23) (green line). Again both lines cannot be distinguished by eye.

The independent potential energy densities $V_x := T_{00,x}^-$ now can be expressed as functions of the scalar densities N_x^s (or N_x^+) instead of the temperature T (and/or quark chemical potential μ_q). For a determination of mean-field potentials for gluons and quarks (antiquarks) it is useful to consider the partonic potential energy density

$$V := T_{00,g}^- + T_{00,q}^- + T_{00,\bar{q}}^- = \tilde{V}_{gg} + \tilde{V}_{qq} + \tilde{V}_{q\bar{q}} \quad (19)$$

and to separate a pure gluonic interaction density \tilde{V}_{gg} from a pure fermionic interaction density \tilde{V}_{qq} as well as a gluon-fermion interaction density $\tilde{V}_{q\bar{q}}$. Correspondingly, a parton density ρ_p and gluon fraction α is defined via

$$\rho_p = N_g^+ + N_q^+ + N_{\bar{q}}^+ , \quad \alpha = \frac{N_g^+}{N_g^+ + N_q^+ + N_{\bar{q}}^+} . \quad (20)$$

In the present DQPM (for $T_c = 0.185$ GeV) the parton density ρ_p (20) turns out to be a simple function of temperature,

$$\rho_p \left(\frac{T}{T_c} \right) \approx \left(\frac{T}{T_c} \right)^{3.15} \quad [\text{fm}^{-3}] , \quad (21)$$

such that the average distance between the partons is given by $d(T/T_c) = \rho_p^{-1/3} \approx (T_c/T)^{1.05}$ [fm] $\approx T_c/T$ [fm]. These relations allow to convert temperatures scales to geometrical scales in a simple fashion.

In Fig. 8 the parton potential energy density V (19) - divided by the parton density ρ_p - is shown as a function of ρ_p (l.h.s.). The functional dependence of V on ρ_p can be well approximated by the expression (cf. l.h.s. of Fig. 8)

$$V(\rho_p) \approx 0.975 \rho_p^{1.292} - 0.71 \rho_p^{-2.1} \quad [\text{GeV}/\text{fm}^3] , \quad (22)$$

where the numbers in front carry a dimension in order to match the units in GeV/fm^3 . The gluon fraction α (20) is shown on the r.h.s. of Fig. 8 and is well approximated by

$$\alpha(\rho_p) = 0.29 - 0.075 \rho_p^{-0.28} - 0.15 \exp(-1.6 \rho_p). \quad (23)$$

Adding half of the interaction density \tilde{V}_{qp} to the gluon part and fermion part separately, we have $T_{00,g}^- = \tilde{V}_{gg} + 0.5\tilde{V}_{gg}$ and $T_{00,q}^- + T_{00,\bar{q}}^- = \tilde{V}_{qq} + 0.5\tilde{V}_{qq}$ such that $\tilde{V}_{qq} - \tilde{V}_{gg} =: \Delta\tilde{V} = T_{00,q}^- + T_{00,\bar{q}}^- - T_{00,g}^-$. The relative fraction of this quantity to the total potential energy density then is evaluated as

$$\kappa(\rho_p) = \frac{\Delta\tilde{V}}{V} = \frac{\Delta\tilde{V}}{T_{00,q}^- + T_{00,\bar{q}}^- + T_{00,g}^-}. \quad (24)$$

Using the *Ansatz*:

$$\tilde{V}_{gg} + \tilde{V}_{qq} = (1 - \xi)V \quad (25)$$

then gives

$$\tilde{V}_{gg} = 0.5(1 - \xi - \kappa)V , \quad \tilde{V}_{qq} = 0.5(1 - \xi + \kappa)V , \quad \tilde{V}_{qp} = \xi V , \quad (26)$$

with still unknown fraction ξ for the interaction density \tilde{V}_{qp} .

In order to determine mean-field potentials $U_g(\rho_p)$ for gluons or $U_q(\rho_p)$ for quarks

(in the rest frame of the system) one has to consider the derivatives (cf. Ref. [35,52])

$$U_g(\rho_p) := \frac{\partial(\tilde{V}_{gg} + \tilde{V}_{qg})}{\partial N_g^+}, \quad U_q(\rho_p) := \frac{\partial(\tilde{V}_{qq} + \tilde{V}_{qg})}{\partial(N_q^+ + N_{\bar{q}}^+)}, \quad (27)$$

which by virtue of (25) can be computed as

$$U_g(\rho_p) = \frac{1}{2} \frac{\partial(1 - \kappa + \xi)V}{\partial \rho_p} \frac{\partial \rho_p}{\partial N_g^+}, \quad U_q(\rho_p) = \frac{1}{2} \frac{\partial(1 + \kappa + \xi)V}{\partial \rho_p} \frac{\partial \rho_p}{\partial(N_q^+ + N_{\bar{q}}^+)}. \quad (28)$$

The fraction ξ of the interaction density - in principle a function of ρ_p but here taken to be a constant - now can be fixed in comparison to the gluon mean-field from Ref. [35] where the pure Yang-Mills sector has been investigated in the same way. This leads to $\xi \approx 0.3$ and separates the total potential energy density V into $\approx 26\%$ for the gluon-gluon interaction part, 30% for the quark-gluon interaction part (including the antiquarks) and $\approx 44\%$ for the fermionic interaction part.

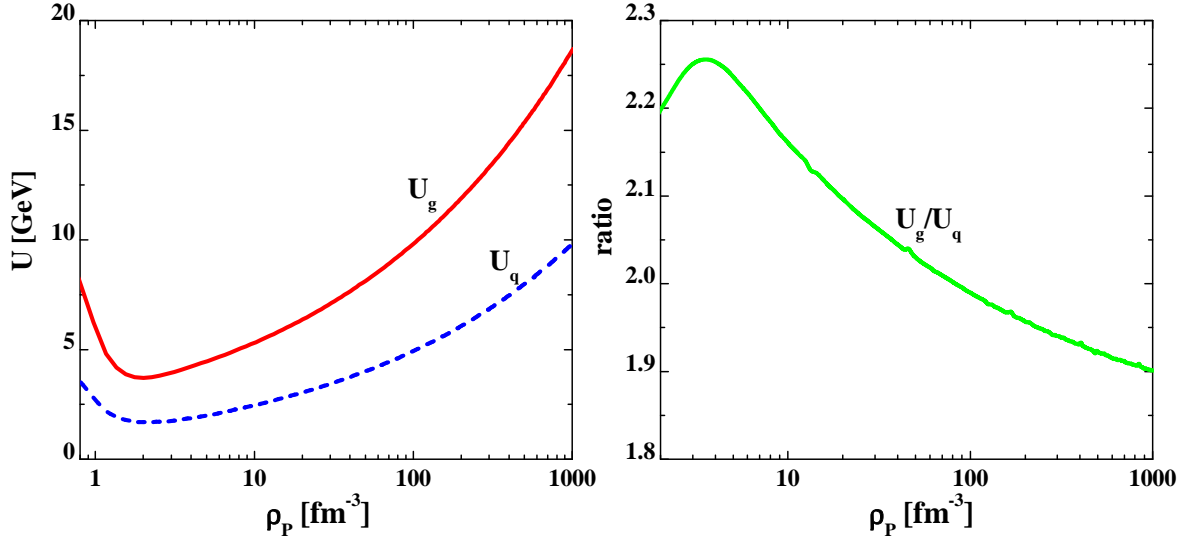


Fig. 9. The mean-field potentials $U_g(\rho_p)$ for gluons (solid red line) and $U_q(\rho_p)$ for quarks (dashed blue line) as a function of the parton density ρ_p (l.h.s.). The r.h.s. displays their ratio as a function of ρ_p which is ≈ 2.05 within 10% accuracy.

The corresponding results for $U_g(\rho_p)$ and $U_q(\rho_p)$ are displayed in the l.h.s. of Fig. 9 in terms of the solid red line and dashed blue line, respectively, and show distinct minima at $\rho_p \approx 2.2 \text{ fm}^{-3}$ which corresponds to an average partonic distance of $\approx 0.77 \text{ fm}$. The actual numerical results for the mean-fields can be fitted by the expressions,

$$U_g(\rho_p) \approx 70 e^{-\rho_p/0.31} + 2.65 \rho_p^{0.21} + 0.45 \rho_p^{0.4} \quad [\text{GeV}], \quad (29)$$

$$U_q(\rho_p) \approx 32 e^{-\rho_p/0.31} + 1.1 \rho_p^{0.21} + 0.3 \rho_p^{0.41} \quad [\text{GeV}],$$

where ρ_p is given in fm^{-3} and the actual numbers in front carry a dimension in order to match to the proper units of GeV for the mean-fields. The ratio $U_g/U_q \approx 2.05$ as can be seen in the r.h.s. of Fig. 9 for a very wide range of parton densities ρ_p within 10% accuracy.

Some comments on the Lorentz structure of the mean fields U_g and U_q appear appropriate. Note that by taking the derivatives with respect to the time-like densities one implicitly assumes that a 4-vector current is the physical source of the selfenergies and that U_g, U_q are the 0'th components of vector fields U_g^ν and U_q^ν ($\nu = 0, 1, 2, 3$). The spatial components are assumed to vanish in the rest frame of the system and can be evaluated by a proper Lorentz boost to the frame of interest. This implies that the dynamical forces (as space-time derivatives of a Lorentz vector) are Lorentz tensors as in case of QED (or vector selfenergies as in the nuclear physics context [52]). On the other hand one might consider the notion of purely scalar selfenergies where derivatives of the potential energy density with respect to the scalar density (e.g. $\partial T_{00,x}^-/\partial N_x^s$) define an effective mass M_x^* [52]. In a selfconsistent framework then the quasiparticles masses (4) should be given by the derivatives with respect to the scalar densities. However, this relation is not fulfilled at all since a numerical evaluation of the scalar derivatives gives effective masses that are larger by more than an order of magnitude as the quasiparticle masses introduced in (4)! This result might have been anticipated since the effective forces for a gauge (vector) field theory should be dominated by Lorentz forces as in case of QED. For completeness we give the fitted expressions for the quasiparticle masses (4) as a function of the scalar densities, respectively,

$$M_g(N_g^s) \approx 0.7(N_g^s)^{0.248} + 0.102(N_g^s)^{-2/3} \quad [\text{GeV}] , \quad (30)$$

$$m_q(N_{q+\bar{q}}^s) \approx 0.36(N_{q+\bar{q}}^s)^{0.257} + 0.14(N_{q+\bar{q}}^s)^{-2/3} \quad [\text{GeV}] ,$$

where the scalar densities are given in units of fm^{-3} and the numbers in front carry a dimension to match the units of GeV for the masses (using $N_{q+\bar{q}}^s = N_q^s + N_{\bar{q}}^s$).

Some information on the properties of the effective gluon-gluon, quark-gluon and quark-quark interaction may be extracted from the second derivatives of the potential energy density V , i.e.

$$v_{gg}(\rho_p) := \frac{\partial^2 \tilde{V}_{gg}}{\partial N_g^{+2}} \approx \frac{1}{2} \frac{\partial^2 (1 - \xi - \kappa)V}{\partial \rho_p^2} \left(\frac{\partial \rho_p}{\partial N_g^+} \right)^2 , \quad (31)$$

$$v_{qq}(\rho_p) := \frac{\partial^2 \tilde{V}_{qq}}{\partial (N_q^+ + N_{\bar{q}}^+)^2} \approx \frac{1}{2} \frac{\partial^2 (1 - \xi + \kappa)V}{\partial \rho_p^2} \left(\frac{\partial \rho_p}{\partial (N_q^+ + N_{\bar{q}}^+)} \right)^2 ,$$

$$v_{qg}(\rho_p) := \frac{\partial^2 \tilde{V}_{qg}}{\partial (N_q^+ + N_{\bar{q}}^+) \partial N_g^+} \approx \frac{\partial^2 (\xi V)}{\partial \rho_p^2} \left(\frac{\partial \rho_p}{\partial (N_q^+ + N_{\bar{q}}^+)} \right) \left(\frac{\partial \rho_p}{\partial N_g^+} \right) .$$

The numerical results for the interactions (31) are displayed in Fig. 10 (l.h.s.) for the effective gluon-gluon (solid red line), gluon-quark (solid blue line) and quark-quark interaction (dashed green line). All interactions show up to become strongly attractive at low parton density $\rho_p < 2.2 \text{ fm}^{-3}$, change sign and become repulsive for all higher parton densities. This situation has been the same in the pure Yang-Mills case [35] (at slightly lower gluon density $\approx 1.4 \text{ fm}^{-3}$). Note that the change of quasiparticle momenta (apart from collisions) will be essentially driven by the (negative) space-derivatives $-\nabla U_j(x) = -dU_j(\rho_p)/d\rho_p \nabla\rho_p(x)$ which implies that the partonic quasiparticles (at low parton density) will bind with decreasing density, i.e. form 'glueballs', mesons, baryons or antibaryons dynamically close to the phase boundary and repel each other for $\rho_p > 2.2 \text{ fm}^{-3}$. Note that color neutrality is imposed by color-current conservation and only acts as a boundary condition for the quantum numbers of the bound/resonant states in color space.

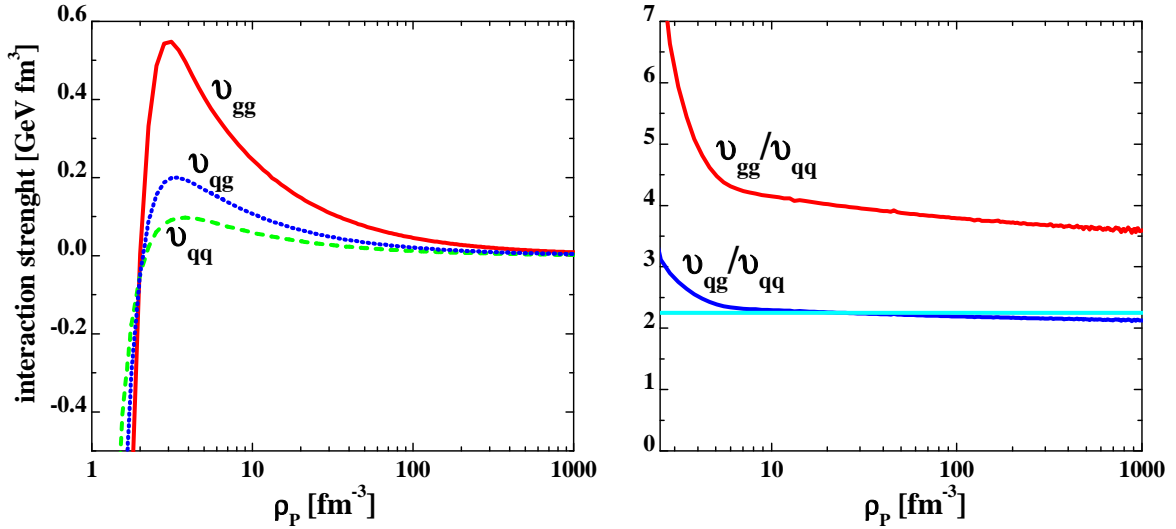


Fig. 10. l.h.s. The effective gluon-gluon (solid red line), gluon-quark (solid blue line) and quark-quark interaction (dashed green line) from the DQPM for $\xi = 0.3$ (see text). The r.h.s. displays the ratios v_{gg}/v_{qq} (solid red line) and v_{qg}/v_{qq} (solid blue line). The straight light blue line is the ratio of the Casimir eigenvalues, i.e. $C_g/C_q = 9/4$.

The r.h.s. of Fig. 10 displays the ratios v_{gg}/v_{qq} (solid red line) and v_{qg}/v_{qq} (solid blue line) as a function of the parton density ρ_p and demonstrates that $v_{qg}/v_{qq} \approx 9/4$, which is the ratio of the Casimir eigenvalues.

A straight forward way to model the parton condensation or clustering to confined glueballs or hadrons dynamically (close to the phase transition) is to adopt screened Coulomb-like potentials $v_c(r, \Lambda)$ with the strength $\int d^3r v_c(r, \Lambda)$ fixed by the interactions $v_{gg}(\rho_p), v_{qg}(\rho_p), v_{qq}(\rho_p)$ from (31) and a screening length Λ from lQCD studies. For the 'dilute parton regime' ($\rho_p < 2.2 \text{ fm}^{-3}$), where two-body interactions should dominate, one may solve a Schrödinger (Dirac or Klein-Gordon) equation for the bound and/or resonant states. This task is not addressed further in the present study since for the actual applications in the PHSD approach [36] the formation of glueballs is discarded and the formation of resonant hadronic states close to the phase

boundary is described by density-dependent transition matrix elements ($\sim |v_{qq}(\rho_p)|^2$) between partons of 'opposite' color with fixed flavor content. In this way the energy-momentum conservation, the flavor current conservation as well as 'color neutrality' are explicitly fulfilled in the (PHSD) transport calculations for interacting particles with spectral functions of finite width.

4 Finite quark chemical potential μ_q

The extension of the DQPM to finite quark chemical potential μ_q is more delicate since a guidance by IQCD is presently very limited. In the simple quasiparticle model one may use the stationarity of the thermodynamic potential with respect to self-energies and (by employing Maxwell relations) derive a partial differential equation for the coupling $g^2(T, \mu_q)$ which may be solved with a suitable boundary condition for $g^2(T, \mu_q = 0)$ [41]. Once $g^2(T, \mu_q)$ is known one can evaluate the changes in the quasiparticle masses with respect to T and μ_q , i.e. $\partial M_x^2/\partial\mu_q$ and $\partial M_x^2/\partial T$ (for $x = g, q, \bar{q}$) and calculate the change in the 'bag pressure' ΔB (cf. Refs. [41,53] for details). However, such a strategy cannot be taken over directly since additionally the quasiparticle widths $\gamma_x(T, \mu_q)$ have to be known in the (T, μ_q) plane in case of the DQPM.

In hard-thermal-loop (HTL) approaches [54,55] the damping of a hard quark (or gluon) does not depend on the quark chemical potential explicitly [57] and one might employ (6) also at finite μ . This, however, has to be considered with care since HTL approaches assume small couplings g^2 and should be applied at sufficiently high temperature, only. Present IQCD calculations suggest that the ratio of pressure to energy density, P/ϵ , is approximately independent on μ_q as a function of the energy density ϵ [56]. Accordingly, the functional dependence of the quasiparticle width γ on μ_q and T has to be modeled in line with 'lattice phenomenology' (see below).

Assuming three light flavors ($q = u, d, s$) and all chemical potentials to be equal ($\mu_u = \mu_d = \mu_s = \mu$) equations (3) and (4) demonstrate that the effective gluon and quark masses are a function of

$$T^{*2} = T^2 + \frac{\mu^2}{\pi^2}. \quad (32)$$

Since the coupling (squared) (5) is a function of T/T_c a straight forward extension of the DQPM to finite μ is to consider the coupling as a function of $T^*/T_c(\mu)$ with a μ -dependent critical temperature,

$$T_c(\mu) \approx T_c(\mu = 0) \left(1 - \frac{1}{2\pi^2} \frac{\mu^2}{T_c(0)^2}\right) \approx T_c(0) \left(1 - 0.05 \frac{\mu^2}{T_c(0)^2}\right). \quad (33)$$

The coefficient in front of the μ^2 -dependent part can be compared to lQCD calculations at finite (but small) μ which gives 0.07(3) [58] instead of 0.05 in (33). Consequently one has to expect an approximate scaling of the DQPM results if the partonic width is assumed to have the form (6),

$$\gamma_g(T, \mu) = N_c \frac{g^2(T^*/T_c(\mu))}{4\pi} T \ln \frac{2c}{g^2(T^*/T_c(\mu))}, \quad (34)$$

$$\gamma_q(T, \mu) = \frac{N_c^2 - 1}{2N_c} \frac{g^2(T^*/T_c(\mu))}{4\pi} T \ln \frac{2c}{g^2(T^*/T_c(\mu))},$$

where $g^2(T/T_c)$ has been replaced by $g^2(T^*/T_c(\mu))$. In fact, as will be demonstrated below, this choice leads to an approximate independence of the potential energies per degree of freedom as a function of μ_q . Nevertheless, the conjecture (34) should be explicitly controlled by lQCD studies for $N_f=3$ at finite quark chemical potential. Unfortunately, this task is presently out of reach and one has to live with the uncertainty in (34) which is assumed in the following investigations.

Within the scaling hypothesis (33), (34) the results for the masses and widths in Section 2.1 stay about the same as a function of $T^*/T_c(\mu)$ when dividing by the temperature T . This also holds approximately when displaying the masses and widths as a function of the parton density ρ_p for different chemical potentials μ as demonstrated in Fig. 11. The latter quantities can well be fitted by the expressions

$$M_g(\rho_p) \approx 0.41 \rho_p^{0.255} + 0.38 \rho_p^{-0.7} \quad [\text{GeV}], \quad (35)$$

$$\gamma_g(\rho_p) \approx 0.235 \rho_p^{0.245} - 0.14 \rho_p^{-2} \quad [\text{GeV}],$$

$$m_q(\rho_p) \approx \frac{2}{3} M_g(\rho_p), \quad \gamma_q(\rho_p) \approx \frac{4}{9} \gamma_g(\rho_p),$$

with ρ_p given in units of fm^{-3} . Note that according to the parametrization (35) the width might become negative for very small ρ_p ; in actual transport applications it should be set to zero in such cases [36].

The more interesting question is how the energy density ϵ (8) and the pressure P (from (7)) change with quark chemical potential $\mu = \mu_q$ in the DQPM. This information is provided in Fig. 12 where the upper l.h.s. shows the energy density ϵ (8) (scaled in terms of $T_{c0} = T_c(\mu = 0) = 0.185 \text{ GeV}$) as a function of $T^*/T_c(\mu)$. Here a scaling of the 'temperature' T^* with $T_c(\mu)$ (33) is used since the phase boundary changes with the quark chemical potential μ . The energy density ϵ is seen to scale well with $(T/T_{c0})^4$ as a function of temperature for $T^*/T_c(\mu) > 3$, however, increases slightly with μ close to the phase boundary where the scaling is violated on the level of 20%. This violation in the scaling (seen in the upper left part of the figure) is essentially due to an increase of the pressure P which is displayed in the lower left

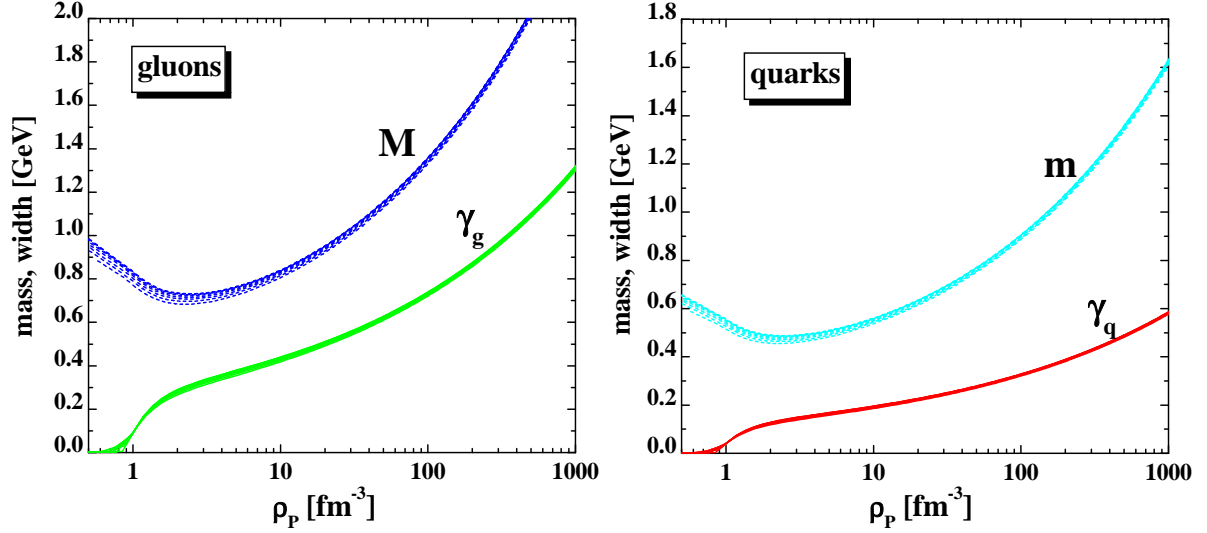


Fig. 11. The gluon mass M and width γ_g (l.h.s.) as a function of the parton density ρ_p for various chemical potentials $\mu_q = \mu$ from $\mu = 0$ to $\mu = 0.21$ GeV in steps of 0.03 GeV. The r.h.s. displays the mass m for quarks and width γ_q for the same quark chemical potentials.

part of the figure as a function of $T^*/T_c(\mu)$ for the same chemical potentials μ from $\mu = 0$ to 0.21 GeV in steps of 0.03 GeV. Note that a quark chemical potential of 0.21 GeV corresponds to a baryon chemical potential of $\mu_B = 3\mu = 0.63$ GeV which is already substantial and the validity of (33) becomes questionable.

Since the pressure P is obtained from an integration of the entropy density s over temperature (7) the increase in P with μ can directly be traced back to a corresponding increase in entropy density. The latter is dominated by the time-like quasiparticle contributions thus 'counting' the effective degrees of freedom,

$$\rho_p = N_g^+ + N_{q+\bar{q}}^+, \quad N_{q+\bar{q}}^+ = N_q^+ + N_{\bar{q}}^+ . \quad (36)$$

The upper r.h.s. of Fig. 12 shows ρ_p versus $T^*/T_c(\mu)$ (multiplied by T_{c0}^3/T^3) for chemical potentials from $\mu = 0$ to $\mu = 0.21$ GeV in steps of 0.03 GeV. Indeed the scaled parton density increases with μ ; this increase is most pronounced for lower temperatures and becomes substantial for $\mu = 0.21$ GeV. One should recall, however, that a tri-critical endpoint (in the T, μ plane) is expected for $\mu_B = 3\mu \approx 0.4$ GeV [59] which corresponds to $\mu \approx 0.13$ GeV. When restricting to the interval $0 \leq \mu \leq 0.13$ GeV the explicit change in the parton density ρ_p with μ stays very moderate. This also holds for the energy density ϵ and the pressure P .

Quite remarkably the potential energy per time-like fermion $T_{00,q+\bar{q}}^-/N_{q+\bar{q}}^+$ changes very little with μ as can be seen from the lower right part of Fig. 12 where the latter quantity is displayed for the same chemical potentials as before (lower green lines) as a function of $T^*/T_c(\mu)$. This also holds for the potential energy per time-like gluon $T_{00,g}^-/N_g^+$ (upper magenta lines). Accordingly the potential energy per time-like degree of freedom is essentially a function of $T^*/T_c(\mu)$ alone.

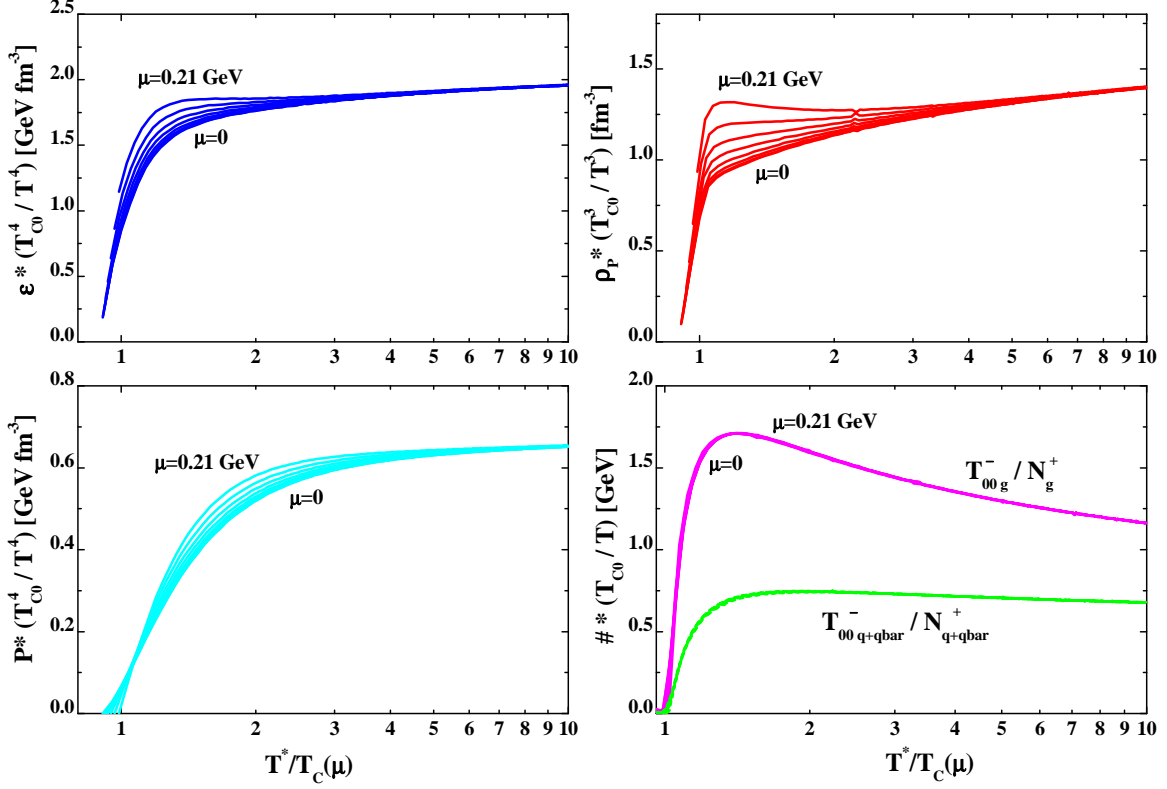


Fig. 12. The energy density $\epsilon(T^*/T_c(\mu))$ (8) for quark chemical potentials μ from 0 to 0.21 GeV in steps of 0.03 GeV as a function of the scaled temperature $T^*/T_c(\mu)$ for $N_f = 3$ (upper l.h.s.). The pressure $P(T^*/T_c(\mu))$ from the thermodynamical relation (7) for quark chemical potentials μ from 0 to 0.21 GeV in steps of 0.03 GeV as a function of the scaled temperature $T^*/T_c(\mu)$ for $N_f = 3$ (lower l.h.s.). The parton density ρ_p (for quark chemical potentials μ from 0 to 0.21 GeV) is shown in the upper r.h.s. The potential energy per time-like 'gluon' (upper magenta lines) and the potential energy per time-like 'quark+antiquark' (lower green lines) for the same quark chemical potentials are displayed in the lower r.h.s. Note that ϵ and P are scaled by the dimensionless factor $(T_{c0}/T)^4$ (with $T_{c0} = 0.185$ GeV) while the parton density ρ_p is scaled by the factor $(T_{c0}/T)^3$.

The time-like densities for the fermions $N_{q+\bar{q}}^+$ (36) (upper l.h.s., dark blue lines) and the space-like quantities $N_{q+\bar{q}}^-$ (upper r.h.s., light blue lines) are shown in Fig. 13 as a function of $T^*/T_c(\mu)$ for chemical potentials μ from $\mu = 0$ to $\mu = 0.21$ GeV in steps of 0.03 GeV (scaled by T_{c0}^3/T^3). Both quantities increase with μ in a comparable fashion such that their ratio stays approximately constant for $T^* > 1.5 T_c(\mu)$. The space-like quantity N_g^- (lower l.h.s., dashed green lines) practically is independent from μ as well as the time-like gluon density N_g^+ (lower l.h.s., red lines). Accordingly the gluon fraction

$$\alpha(T, \mu) = \frac{N_g^+}{N_g^+ + N_{q+\bar{q}}^+}, \quad (37)$$

which is displayed on the lower r.h.s. of Fig. 13 for the same set of quark chemical

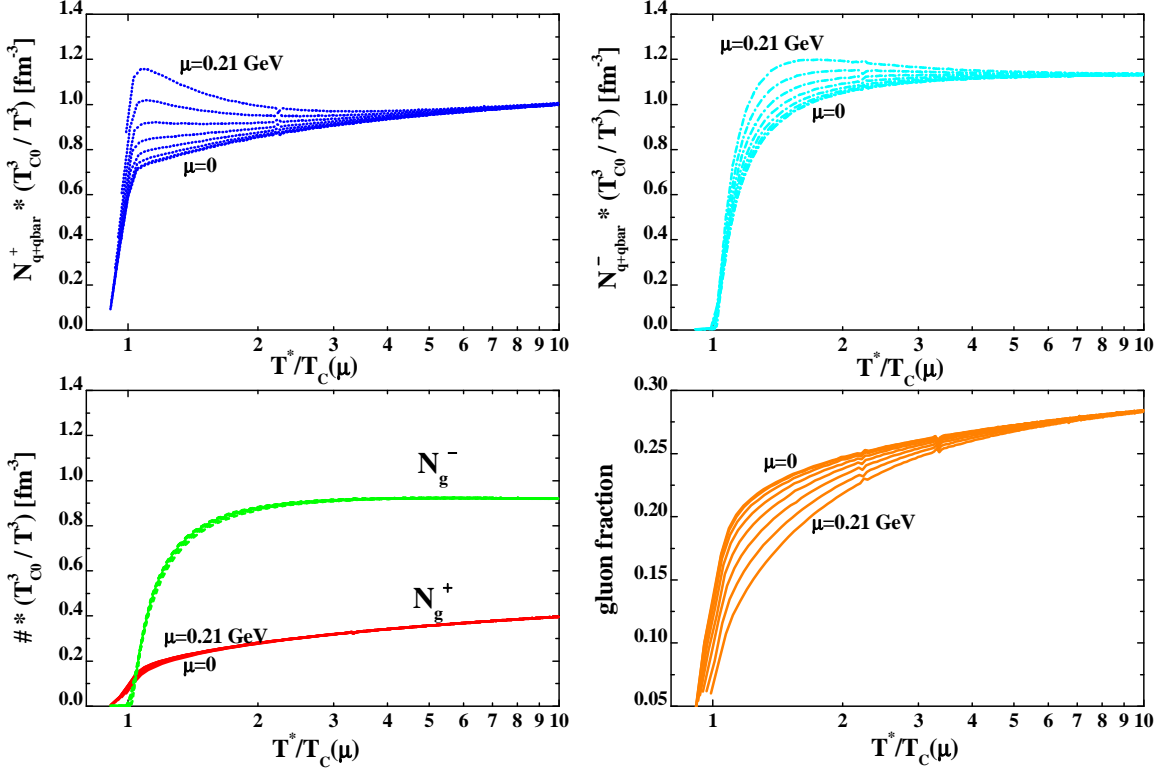


Fig. 13. Upper parts: The time-like fermion density $N_{q+\bar{q}}^+$ (l.h.s., dark blue lines) and the space-like quantity $N_{q+\bar{q}}^-$ (r.h.s., light blue lines) for quark chemical potentials μ from 0 to 0.21 GeV in steps of 0.03 GeV as a function of the scaled temperature $T^*/T_c(\mu)$. Lower parts: the time-like gluon density N_g^+ (l.h.s., lower red lines) and the space-like quantity N_g^- (l.h.s., dashed green lines) for the same quark chemical potentials as a function of $T^*/T_c(\mu)$. Both, N_g^- and N_g^+ change only very little with μ in the whole temperature range; the relative changes are of the order of the line width. The gluon fraction (37) is shown on the r.h.s. as a function of the scaled temperature $T^*/T_c(\mu)$ for quark chemical potentials μ from 0 to 0.21 GeV in steps of 0.03 GeV. Note that all 'densities' have been multiplied by the dimensionless factor $(T_{c0}/T)^3$.

potentials as a function of $T^*/T_c(\mu)$, decreases with μ . It drops to zero below the phase boundary because the difference between the gluon effective mass and the fermion effective mass becomes large below T_c .

We continue with the time-like and space-like energy densities for the fermions and gluons as a function of μ and $T^*/T_c(\mu)$ which are displayed on the l.h.s. of Fig. 14. The upper part shows that the space-like and time-like energy densities for the fermions increase with μ roughly in a similar fashion as the fermion 'densities' such that their ratio is approximately independent on μ . The lower part of Fig. 14 (l.h.s.) indicates that the space-like energy density for gluons (green lines) as well as the time-like energy density for gluons (red lines) are approximately independent from μ within line width. When separating the time-like fermion energy density into contributions from quarks q and antiquarks \bar{q} (r.h.s. of Fig. 14) we find an increase of $T_{00,q}^+$ with μ which is not fully compensated by a decrease of $T_{00,\bar{q}}^+$ with quark chemical potential.

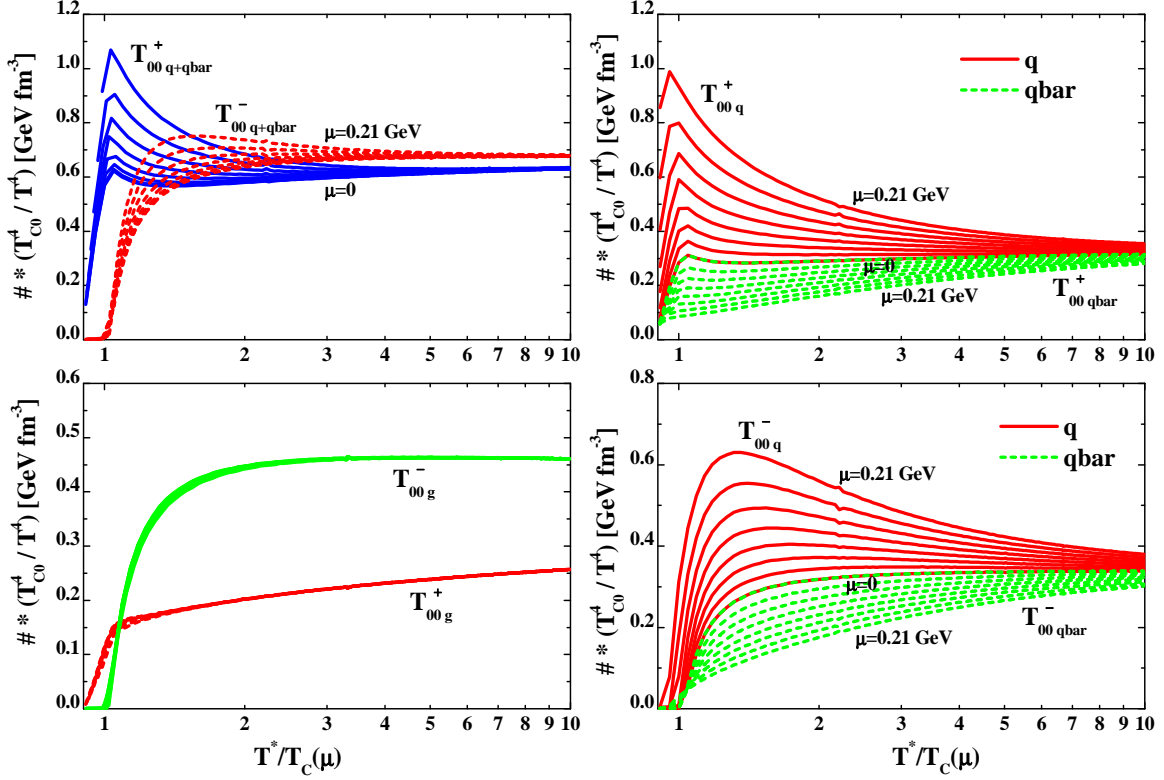


Fig. 14. l.h.s.: The time-like fermion energy density $T_{00,q+\bar{q}}^+$ (blue lines) and the space-like fermion energy density $T_{00,q+\bar{q}}^-$ (dashed red lines) for quark chemical potentials μ from 0 to 0.21 GeV in steps of 0.03 GeV as a function of the scaled temperature $T^*/T_c(\mu)$ (upper l.h.s.). The lower l.h.s. shows the time-like (dashed red lines) and space-like gluon energy density (green lines) for the same chemical potentials as a function of the scaled temperature. Both, $T_{00,g}^-$ and $T_{00,g}^+$ are roughly independent from μ in the whole temperature range. The time-like (upper r.h.s) and space-like energy densities (lower r.h.s.) for quarks (upper red lines) and antiquarks (lower green lines) are separately displayed for quark chemical potentials μ from 0 to 0.21 GeV in steps of 0.03 GeV for $N_f = 3$. All quantities have been multiplied by the dimensionless factor T_{c0}^4/T^4 .

Similar dependences on μ and T^* are found for the space-like sector (lower part, r.h.s.). Thus when summing up all space-like and time-like energy densities from the fermions and the gluons a small net increase in the total energy density with μ survives (see also upper left part of Fig. 12).

We note in passing that derivatives of the various energy densities w.r.t. the time-like gluon or fermion densities (as investigated in detail in Section 3) are approximately independent of μ such that the effective potentials $U_g(\rho_p)$, $U_q(\rho_p)$ and $U_{\bar{q}}(\rho_p)$ (28) stay practically the same. Since this result may be inferred already from the μ -(in)-dependence of the potential energy per time-like degree of freedom (displayed in the lower r.h.s. of Fig. 12) an explicit representation is discarded. This implies that the mean-fields (28) or parametrizations (29) may be employed also at finite (moderate) net quark density $N_q^+ - N_{\bar{q}}^+$ which simplifies an implementation in parton transport models (as e.g. PHSD).

Whereas for vanishing quark chemical potential $\mu=0$ the quark and antiquark densities are the same this no longer holds for finite μ where the differences

$$\rho_q^\pm = N_q^\pm - N_{\bar{q}}^\pm \quad (38)$$

are of separate interest since $\rho_q = \rho_q^+ + \rho_q^-$ is the zero'th component of a conserved flavor current (separately for each flavor u, d, s, \dots). In order to obtain some idea about space-like and time-like contributions of the net quark density ρ_q in the DQPM we first plot the time-like component ρ_q^+ in the l.h.s. of Fig. 15 as a function of $T^*/T_c(\mu)$ for different μ from 0 to 0.3 GeV (as before). In order to divide out the leading scaling with temperature the time-like densities have been multiplied by T_{c0}^2/T^2 on the l.h.s. of Fig. 15 (as known from Fermi systems in the nuclear physics context). The actual results show an approximately linear increase in μ (l.h.s.) which suggests to study the scaled quantities $\rho_q^\pm \cdot T_{c0}^2/(\mu T^2)$. However, a better scaling is obtained when multiplying ρ_q^\pm by $T_{c0}^2/(\mu T^{*2})$. The latter quantities are displayed in the r.h.s. of Fig. 15 for the same set of chemical potentials as before. This approximate scaling allows to estimate the net quark density as

$$\rho_q \approx 10 \mu T^{*2}/T_{c0}^2 \text{ [fm}^{-3}\text{]} \quad (39)$$

with μ given in units of GeV in case of $N_f = 3$.

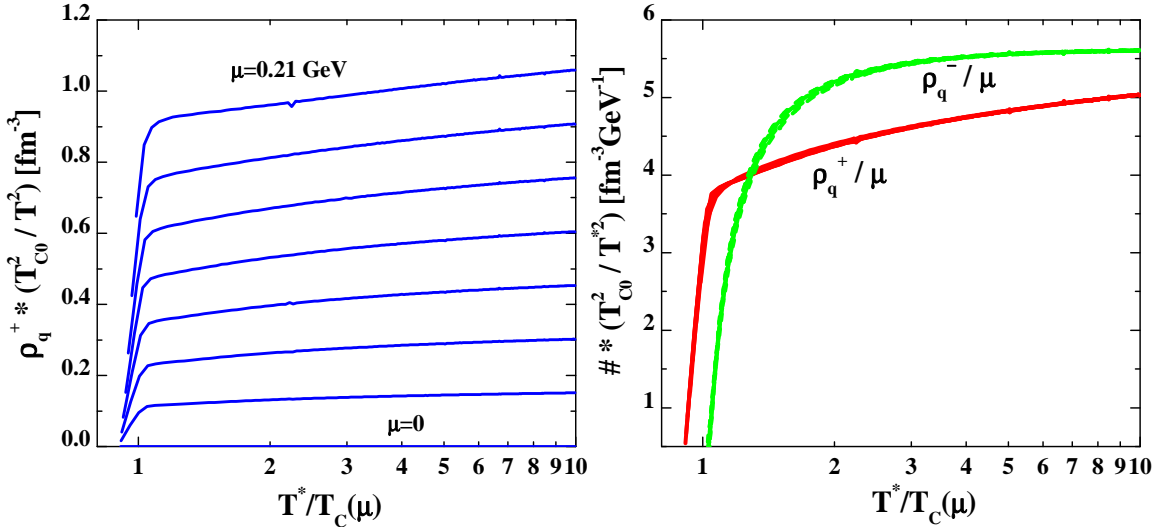


Fig. 15. l.h.s.: The time-like quark density ρ_q^+ (38) (scaled by the dimensionless factor T_{c0}^2/T^2) for quark chemical potentials μ from 0 to 0.21 GeV in steps of 0.03 GeV as a function of the scaled temperature $T^*/T_c(\mu)$. r.h.s.: The time-like quark density ρ_q^+ (38) (red solid lines) and the space-like quantity ρ_q^- (38) (dashed green lines) for the same quark chemical potentials μ . In this part of the figure all quantities are scaled by the factor $T_{c0}^2/T^{*2}/\mu$.

The approximate scaling depicted in Fig. 15 is a prediction of the DQPM in case of 3 quark flavors and should be controlled by IQCD calculations. For two light flavors

($N_f = 2$) some comparison can be made in the low temperature (and low μ) range. Unfortunately the simple scaling relation (39) does not hold at small T such that an explicit comparison has to be presented between the DQPM for $N_f = 2$ and the IQCD calculations from Ref. [60]. The latter calculations have been carried out on a $16^3 \times 4$ lattice with two continuum flavors (of p4-improved staggered fermions) with mass $m = 0.4T$. Though the fermion masses are not really 'light' in the IQCD calculations the actual IQCD results may serve a test of the present DQPM in the 2-flavor sector (for low μ and T). The explicit IQCD results for the net quark density ρ_q (divided by T^3) are displayed in Fig. 16 as a function of T/T_{c0} in terms of the various symbols. The symbols of equal color correspond to $\mu/T_{c0} = 1.0, 0.8, 0.6, 0.4,$ and 0.2 from top to bottom and by eye show an approximately linear dependence on μ . The explicit results from the DQPM for $N_f = 2$ are presented in terms of the dark green lines and approximately follow the IQCD results (at least for smaller μ). Since the systematic errors of the IQCD calculations are not known to the author an explicit refitting of the parameters $\lambda, T_s/T_c$ and c for $N_f = 2$ (cf. Section 2.1) is discarded here. Nevertheless, the qualitative (and partly quantitative) agreement between the DQPM and IQCD provides a test for the basic concepts of the DQPM.

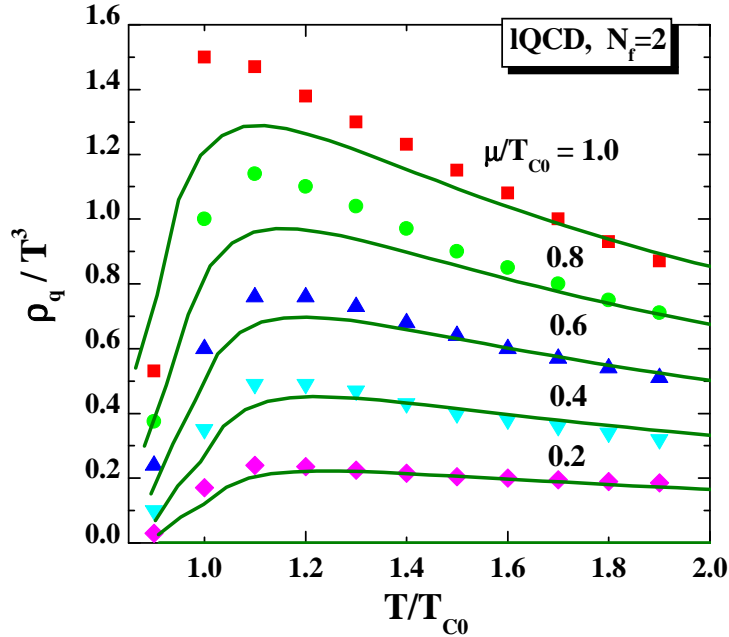


Fig. 16. The quark density ρ_q (38) (divided by the factor T^3) for quark chemical potentials μ/T_{c0} from 0 to 1.0 in steps of 0.2 as a function of the scaled temperature T/T_{c0} from the DQPM (green lines) for $N_f = 2$. The different symbols represent the IQCD results from Ref. [60] for the same quark chemical potentials as a function of T/T_{c0} (also for $N_f = 2$). Note that the temperature axis here is given by $T/T_{c0} = T/T_c(\mu = 0)$ and not by $T^*/T_c(\mu)$!

5 Dilepton radiation from the sQGP

The properties of the sQGP so far have been fixed in the DQPM by specifying the (vector) selfenergies/potentials as well as effective interactions for the time-like partons. As shown in Ref. [6] this leads to a strongly interacting partonic system with a shear viscosity to entropy density ratio close to $\eta/s \approx 0.2$. However, the predictions from the DQPM should be controlled by independent lQCD studies to get some idea about the reliability of the approach. As mentioned before transport coefficients like the shear viscosity η are available from lQCD [18] but the present accuracy is not satisfactory. On the other hand some lQCD information is available from the Bielefeld group on the electromagnetic correlator which is intimately related to the dilepton emission rate [61–63].

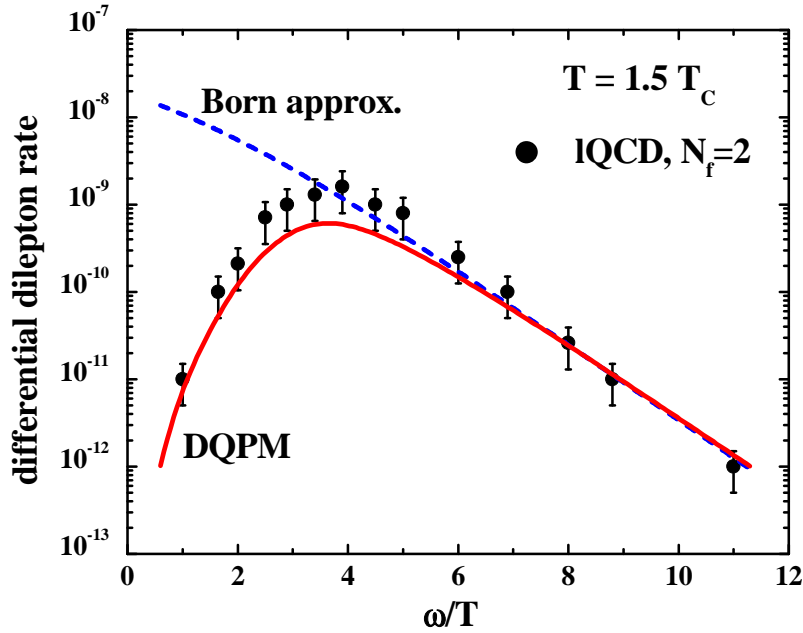


Fig. 17. The 'back-to-back' dilepton emission rate (41) from the DQPM (solid red line) in comparison to the Born approximation (40) for massless partons (dashed blue line) and the results from the lQCD analysis in Ref. [63] at $T = 1.5 T_c$ in case of $N_f = 2$ (full dots).

In order to provide some further comparison to lQCD results we consider the dilepton production rate in thermal equilibrium (at temperature T) in a two-flavor QGP as in Ref. [63]. For massless quarks and antiquarks the emission rate of 'back-to-back' leptons (e^+e^-) is given by [63,64]

$$\frac{dW}{d\omega d^3p}(\mathbf{p} = 0) = \frac{5\alpha^2}{36\pi^4} n_F\left(\frac{\omega}{2T}\right) n_F\left(\frac{\omega}{2T}\right), \quad (40)$$

where ω is the invariant mass of the lepton pair and n_F denotes the Fermi distribution function. In (40) α is the electromagnetic coupling constant. For massless partons, furthermore, the magnitude of the lepton momenta is given by $|\mathbf{p}| = \omega/2$ while their

direction is opposite in the dilepton rest frame. Neglecting the rest mass of leptons their energy is $\omega/2$ in the dilepton rest frame, too. The expression (40) changes in case of spectral functions with finite width to

$$\frac{dW}{d\omega d^3p} = \frac{5\alpha^2}{36\pi^4} \int_0^\infty d\omega_1 \int_0^\infty d\omega_2 \int_0^\infty dp \frac{\omega_1 \omega_2}{\pi \pi} \rho_q(\omega_1, p; T) \rho_{\bar{q}}(\omega_2, p; T) \quad (41)$$

$$\cdot \frac{\sqrt{\tilde{\lambda}(\omega^2, P_1^2, P_2^2)}}{\omega^2} \delta(\omega - \omega_1 - \omega_2) n_F\left(\frac{\omega_1}{T}\right) n_F\left(\frac{\omega_2}{T}\right)$$

with $P_j^2 = \omega_j^2 - p^2$ denoting the invariant mass of the annihilating partons $j = 1, 2$. In (41) the factor $\sqrt{\tilde{\lambda}}/\omega^2$ gives a flux correction in case of massive quasiparticles with $\tilde{\lambda}(x, y, z) = (x - y - z)^2 - 4yz$.

Since the spectral functions in the DQPM are fixed (cf. Section 2) the lepton emission rate (41) can be evaluated without introducing any further assumption (or parameter). The results for the different emission rate for $N_f = 2$ are shown in Fig. 17 for $T = 1.5 T_c$ (solid red line) in comparison to the limit (40) (dashed blue line) and the lQCD results from [63] (full dots). The lQCD dilepton rate has been obtained from the temporal correlators in lQCD employing the 'maximum entropy method' which has a systematic error in the order of 30 to 50 % [63] depending on the energy scale considered. The results from Fig. 17 demonstrate a drastic suppression of low mass lepton pairs due to the finite mass of the partons. On the other hand the spectra from the DQPM are in qualitative agreement with the lQCD results from Ref. [63] when including the systematic uncertainties of the latter approach. Thus the DQPM (in its present version) passes a further test in comparison to lQCD.

6 Conclusions and discussion

The present study has provided a novel interpretation of the dynamical quasiparticle model (DQPM) by separating time-like and space-like quantities for particle densities, energy densities, entropy densities ect. that also paves the way for an off-shell transport approach [36]. As known from previous studies [34,35] the entropy density s is found to be dominated by the on-shell quasiparticle contribution while the space-like part of the off-shell contribution gives only a small (but important) enhancement. However, in case of the parton 'densities' $N_x = N_x^+ + N_x^-$ and the energy densities $T_{00,x} = T_{00,x}^+ + T_{00,x}^-$ ($x = g, q, \bar{q}$) the situation is opposite: here the space-like parts ($N_x^-, T_{00,x}^-$) dominate over the time-like parts ($N_x^+, T_{00,x}^+$) except close to T_c where the independent quasiparticle limit of on-shell particles is approximately regained. The latter limit is a direct consequence of the infrared enhancement of the coupling (5) close to T_c (in line with the lQCD studies in Ref. [44]) and a decrease of the width γ (6) when approaching T_c from above.

Since only the time-like part of the parton density can be propagated within the lightcone the space-like part N_x^- has to be attributed to t -channel exchange partons in scattering processes that contribute also to the space-like energy densities $T_{00,x}^-$. The latter quantities may be regarded as potential energy densities V_x . This, in fact, is legitimate since the total quasiparticle energy density T^{00} (16) very well matches the energy density (8) obtained from the thermodynamical relations. Only small deviations indicate that the DQPM in its straightforward application is not fully consistent in the thermodynamical sense.

By taking derivatives of the potential energy densities V_x with respect to the time-like gluon and fermion densities one may deduce mean-field potentials U_x for gluons and quarks (antiquarks) as a function of the parton density ρ_p which enters instead of the thermodynamical Lagrange parameters T and μ_q . Second derivatives w.r.t. the gluon and/or fermion densities then define effective interactions between gluons, quarks and quarks and gluons. We find that the gluon-gluon interaction is stronger than the quark-quark (antiquark) by roughly a factor of 4-5 whereas the quark-gluon interaction strength approximately scales (relative to the quark-quark interaction) by the ratio of Casimir eigenvalues, i.e. $9/4$. The effective parton-parton interactions are repulsive for $\rho_p > 2.2 \text{ fm}^{-3}$ and turn strongly attractive at lower density. Since at low parton densities (or average distances larger than 0.77 fm) the system may be described by 2- and 3-body dynamics the strong attraction will lead to color neutral bound states of gluons (glueballs), quark and antiquarks (mesons) as well as 3 quarks or 3 antiquarks (baryons or antibaryons). The mean-field potentials U_x are found to be independent on the quark chemical potentials μ_q (within 5%) such that the respective analytical approximations (29) are well suited for an implementation in off-shell parton transport approaches (as e.g. PHSD).

Since for the case of three light flavors ($N_f=3$) the effective masses (squared) in the DQPM scale with $T^{*2} := T^2 + \mu_q^2/\pi^2$ and the spectral width of the dynamical quasiparticles is assumed to be given by the 'modified' HTL expression (34) an approximate scaling of various quantities is found in the DQPM at finite quark chemical potential μ_q . As an example we find that the potential energy per time-like gluon as well as the potential energy per time-like fermion are approximately independent on μ_q which directly leads to the independence of the mean-fields U_x on μ_q (as mentioned above). Furthermore the net quark density is found to roughly scale as $\rho_q \sim \mu_q T^{*2}$ which might be directly checked by lQCD. In addition the energy density ϵ and the pressure P are found to increase only slightly with μ_q close to T_c such that the ratio P/ϵ (as a function of ϵ) is also approximately independent on μ_q .

Explicit comparisons of the DQPM calculations with lQCD results have been performed for the sound velocity (squared) (10) in the 2+1 flavor case and in the two flavor sector ($N_f=2$) for the net quark density as a function of temperature T and μ_q from [60]. The results are in an acceptable agreement such that the DQPM - which presently has been fixed only in the pure Yang-Mills sector ($N_f=0$) - reproduces the dominant dependences on T and μ_q . Furthermore, it could be shown that the 'back-

to-back' dilepton emission rate from the DQPM in case of $N_f=2$ is in qualitative agreement with IQCD studies from Ref. [63] at $T = 1.5 T_c$ thus providing a further independent test of the model. Note that in a conventional quasiparticle model with vanishing width γ_q the dilepton emission rate only gives contributions for invariant masses above $2 m_q$ which is not in line with the IQCD result from Ref. [63].

Some note of caution with respect to the present DQPM appears appropriate: the parameters in the effective coupling (5) and the width (6) have been fixed in the DQPM by the entropy (1) to IQCD results for $N_f=0$ assuming the form (2) for the spectral function $\rho(\omega)$. Alternative assumptions for $\rho(\omega)$ will lead to slightly different results for the time-like and space-like densities, energy densities *etc.* but not to a qualitatively different picture. Also it is presently unclear if the three parameters $(\lambda, T_s/T_c, c)$ employed in Section 2.1 are approximately the same in case of two or three dynamical flavors. More precise calculations from IQCD should allow to put further constraints on the form of the spectral function $\rho(\omega)$ and to fix the basic model parameters in the effective coupling. Also the 'modified' HTL expression (34) for the quasiparticle width has to be controlled by IQCD at finite μ_q as well as transport coefficients like the shear viscosity η or related correlators.

The author acknowledges valuable discussions with E. L. Bratkovskaya, M. H. Thoma and A. Peshier.

References

- [1] M. Tannenbaum, *nucl-ex/0702028*.
- [2] P. Jacobs, D. Kharzeev, B. Müller, J. Nagle, K. Rajagopal, S. Vigdor, *nucl-ex/07051930*.
- [3] *Quark Matter 2002*, Nucl. Phys. A 715 (2003) 1; *Quark Matter 2004*, J. Phys. G 30 (2004) S633; *Quark Matter 2005*, Nucl. Phys. A 774 (2006) 1.
- [4] F. Karsch *et al.*, Nucl. Phys. B 502 (2001) 321.
- [5] M. H. Thoma, J. Phys. G 31 (2005) L7; Nucl. Phys. A 774 (2006) 307.
- [6] A. Peshier, W. Cassing, Phys. Rev. Lett. 94 (2005) 172301.
- [7] E. Shuryak, Prog. Part. Nucl. Phys. 53 (2004) 273.
- [8] I. Arsene *et al.*, Nucl. Phys. A 757 (2005) 1; B. B. Back *et al.*, Nucl. Phys. A 757 (2005) 28; J. Adams *et al.*, Nucl. Phys. A 757 (2005) 102; K. Adcox *et al.*, Nucl. Phys. A 757 (2005) 184.
- [9] T. Hirano, M. Gyulassy, Nucl. Phys. A 769 (2006) 71.
- [10] W. Cassing, K. Gallmeister, C. Greiner, Nucl. Phys. A 735 (2004) 277.

- [11] E. L. Bratkovskaya *et al.*, Phys. Rev. C 67 (2003) 054905; Phys. Rev. C 69 (2004) 054907; Phys. Rev. C 71 (2005) 044901.
- [12] K. Gallmeister, W. Cassing, Nucl. Phys. A748 (2005) 241.
- [13] P. Kolb, U. Heinz, nucl-th/0305084, in 'Quark Gluon Plasma 3', Eds. R. C. Hwa, X.-N. Wang, World Scientific, Singapore, 2004.
- [14] C. Nonaka, S. A. Bass, Phys. Rev. C 75 (2007) 014902; Nucl. Phys. A 774 (2006) 873.
- [15] G. E. Brown, C.-H. Lee, M. Rho, E. Shuryak, Nucl. Phys. A740 (2004) 171.
- [16] G. E. Brown, C.-H. Lee, M. Rho, Nucl. Phys. A 747 (2005) 530.
- [17] E. V. Shuryak, I. Zahed, Phys. Rev. D 70 (2004) 054507.
- [18] A. Nakamura, S. Sakai, Phys. Rev. Lett. 94 (2005) 072305; Nucl. Phys. A 774 (2006) 775.
- [19] B. Zhang, L.-W. Chen, C. M. Ko, arXiv: 0705.3968 [nucl-th].
- [20] E. L. Bratkovskaya, W. Cassing, Nucl. Phys. A 619 (1997) 413; W. Cassing, E. L. Bratkovskaya, Phys. Rep. 308 (1999) 65.
- [21] S.A. Bass *et al.*, Prog. Part. Nucl. Phys. 42 (1998) 279.
- [22] M. Bleicher *et al.*, J. Phys. G 25 (1999) 1859.
- [23] K. Geiger, Phys. Rep. 258 (1995) 237.
- [24] B. Zhang, M. Gyulassy, C. M. Ko, Phys. Lett. B 455 (1999) 45.
- [25] D. Molnar, M. Gyulassy, Phys. Rev. C 62 (2000) 054907; Nucl. Phys. A 697 (2002) 495; Nucl. Phys. A 698 (2002) 379.
- [26] S. A. Bass, B. Müller, D. K. Srivastava, Phys. Lett. B 551 (2003) 277; Acta Phys. Hung. A 24 (2005) 45.
- [27] Z.-W. Lin *et al.*, Phys. Rev. C 72 (2005) 064901.
- [28] Z. Xu, C. Greiner, Phys. Rev. C 71 (2005) 064901; Z. Xu, C. Greiner, Nucl. Phys. A 774 (2006) 034909.
- [29] W. Cassing, S. Juchem, Nucl. Phys. A 665 (2000) 377; W. Cassing, S. Juchem, Nucl. Phys. A 672 (2000) 417.
- [30] S. Juchem, W. Cassing, C. Greiner, Phys. Rev. D 69 (2004) 025006; Nucl. Phys. A 743 (2004) 92.
- [31] S. Leupold, Nucl. Phys. A 672 (2000) 475.
- [32] W. Cassing, L. Tolos, E. L. Bratkovskaya, A. Ramos, Nucl. Phys. A 727 (2003) 59.
- [33] A. Peshier, Phys. Rev. D 70 (2004) 034016.
- [34] A. Peshier, J. Phys. G 31 (2005) S371.

- [35] W. Cassing, Nucl. Phys. A 791 (2007) 365.
- [36] W. Cassing, talk at ECT*, Workshop on *Parton Propagation through Strongly Interacting Matter*, September 27, 2005, [<http://conferences.jlab.org/ECT/program>].
- [37] I. C. Arsene *et al.*, Phys. Rev. C 75 (2007) 034902.
- [38] E. Riedel, Z. Phys. 210 (1968) 403.
- [39] B. Vanderheyden, G. Baym, J. Stat. Phys. 93 (1998) 843.
- [40] J.-P. Blaizot, E. Iancu, A. Rebhan, Phys. Rev. Lett. 83 (1999) 2906; Phys. Rev. D 63 (2001) 065003.
- [41] A. Peshier, B. Kämpfer, O. P. Pavlenko, G. Soff, Phys. Rev. D 54 (1996) 2399; P. Levai, U. Heinz, Phys. Rev. C 57 (1998) 1879; A. Peshier, B. Kämpfer, G. Soff, Phys. Rev. C 61 (2000) 045203, Phys. Rev. D 66 (2002) 094003.
- [42] M. Bluhm, B. Kämpfer, R. Schulze, D. Seipt, U. Heinz, arXiv:0705.0397 [hep-ph].
- [43] J. Letessier, J. Rafelski, Phys. Rev. C 67 (2003) 031902.
- [44] O. Kaczmarek, F. Karsch, F. Zantow, P. Petreczky, Phys. Rev. D 70 (2004) 074505; erratum-ibid. D 72 (2005) 059903.
- [45] R. D. Pisarski, Phys. Rev. Lett. 63 (1989) 1129; V. V. Lebedev, A. V. Smilga, Ann. Phys. (N.Y.) 202 (1990) 229.
- [46] F. Karsch, Nucl. Phys. A 698 (2002) 199c; F. Karsch, E. Laermann, A. Peikert, Phys. Lett. B 478 (2000) 447.
- [47] M. Cheng *et al.*, Phys. Rev. D 74 (2006) 054507.
- [48] Y. Aoki, Z. Fodor, S. D. Katz, K. K. Szabo, Phys. Lett. B 643 (2006) 46.
- [49] A. Peshier, Phys. Rev. D 63 (2001) 105004.
- [50] Y. Aoki, Z. Fodor, S. D. Katz, K. K. Szabo, arXiv:hep-lat/0510084, JHEP 0601 (2006) 089.
- [51] Yu.B. Ivanov, V.V. Skolov, V.D. Toneev, Phys. Rev. D 71 (2005) 014005.
- [52] B. D. Serot, J. D. Walecka, Adv. Nucl. Phys. 16 (1986) 1; B. D. Serot, Rep. Prog. Phys. 55 (1992) 1855; P. G. Reinhard, Rep. Prog. Phys. 52 (1989) 439.
- [53] A. Rebhan, P. Romatschke, Phys. Rev. D 68 (2003) 025022.
- [54] E. Braten, R. D. Pisarski, Phys. Rev. D 45 (1992) 1827.
- [55] J. P. Blaizot, E. Iancu, Nucl. Phys. B 417 (1994) 608.
- [56] Z. Fodor, S. D. Katz, K. K. Szabo, Phys. Lett. B 568 (2003) 73.
- [57] H. Vija, M. H. Thoma, Phys. Lett. B 342 (1995) 212.
- [58] C. R. Allton *et al.*, Phys. Rev. D 66 (2002) 074507.

- [59] F. Csikor, G. I. Egri, Z. Fodor, S. D. Katz, K. K. Szabo, A. I. Toth, Prog. Theor. Phys. Suppl. 153 (2004) 93.
- [60] C. R. Allton *et al.*, Phys. Rev. D 68 (2003) 014507.
- [61] R. Rapp, J. Wambach, Adv. Nucl. Phys. 25 (2000) 1.
- [62] F. Karsch, M. G. Mustafa, M. H. Thoma, Phys. Lett. B 497 (2001) 249.
- [63] F. Karsch, E. Laermann, P. Petreczky, S. Stickan, I. Wetzorke, Phys. Lett. B 530 (2002) 147.
- [64] E. Braten, R. D. Pisarski, T. C. Yuan, Phys. Rev. Lett. 64 (1990) 2242.